Chapter 3

Interplay between Short-Chain and Long-Chain Branches

3.1 INTRODUCTION

The ultimate physical properties of semicrystalline materials are directly related to their molecular characteristics. For example, a strong, opaque plastic bin and flexible, transparent wrap can be made from materials having identical chemical formulas. However, the molecular architecture of plastic wrap is quite different and is composed of many short-chain and long-chain branches; in comparison, the molecular architecture of the plastic bin is primarily branch-free.

Long-chain branches (LCB) are well known to affect the melt dynamics of a polymer,[1, 2] which becomes exceedingly important when semicrystalline materials are exposed to flow during processing.[3-5] Based on their relaxation rates, molecules in a flow field will be perturbed from their equilibrium configuration by varying degrees, sometimes resulting in the formation of oriented crystal nuclei.[6, 7] These thread-like precursors result in increased nucleation density and serve as a template for the formation of an oriented morphology with increased crystallization kinetics.[8-12] LCB materials provide an ideal system to probe the effects of melt dynamics because they relax through a hierarchy of motions;[13] for example, an H-polymer exhibits two relaxation processes—that of the arms followed by that of the backbone.[14] Systematic variation of melt relaxation times can be achieved through the synthesis of well-defined materials with controlled lengths and amounts of long-chain branching.

On an industrial scale, long-chain branched molecules can be synthesized using metallocene catalyst technology, which allows the incorporation of branches into the chain during polymerization.[5, 15-19] However, the resulting materials are far from monodisperse ($M_w/M_n > 2$) and the LCB content is not precisely controlled.[2, 20] Additionally,

metallocene materials have been found to contain a small amount of interchain and intrachain heterogeneities, leading to distributions of branches that are not entirely random.[21] In contrast, anionic polymerization followed by hydrogenation allows for the synthesis of fairly monodisperse ($M_w/M_n < 1.1$) polyethylene molecules of well-defined architecture, such as star, H-, pom-pom, and comb polymers, similar to the ones used in this work.[22-26] These model polyethylenes were initially thought to be ideal systems for studies regarding melt dynamics.[3] However, in addition to long-chain branches, short-chain branching (SCB) are also incorporated into the chain; during the polymerization, a minimum 8% of the ethylene addition is 1,2 versus the standard 1,4 addition, resulting in a random distribution of ethyl side groups (Figure 3.1).[27, 28] The resulting molecules are termed hydrogenated polybutadienes (HPBDs) because they are chemically equivalent to random, homogeneous ethylene-co-butene copolymers with a minimum of 7 wt % butene.

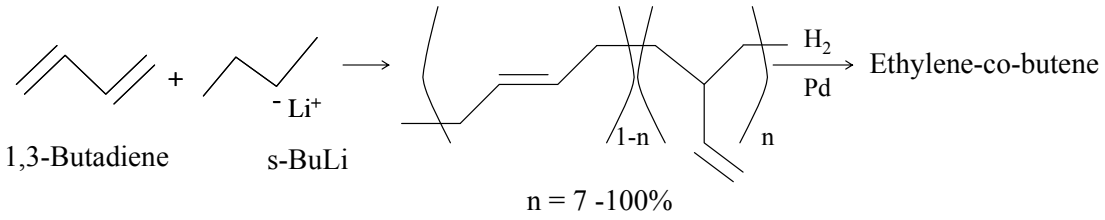

Figure 3.1 HPBD synthesis via anionic polymerization followed by hydrogenation.

The presence of short-chain branches complicates the application of HPBD materials to probe melt dynamics since LCB effects must be isolated from SCB effects. On the other hand, these model systems allow for well-defined studies of the interplay between long-chain and short-chain branches. These systems can be used to gain further understanding of highly industrially-relevant materials like low density polyethylene (LDPE), which contains many short-chain and long-chain branches and is used abundantly for all-purpose containers, machinable plastic parts, and computer components.

Short-chain branches directly affect crystallinity and have very pronounced effects on the structure and properties of semicrystalline materials,[29-32] spurring investigations of linear, homogenous copolymers. The presence of short-chain branches results in increased flexibility and toughness as a consequence of decreased crystallinity.[29, 30, 33-35] The melting point decreases with increasing SCB content due to decreased crystal size,[4, 36, 37] which leads to a deteriorated morphology. [30, 32, 37, 38] Under quiescent conditions, molecules with increased SCB content form thinner lamellae with decreased lateral dimensions and lose the ability to organize into super-molecular structures, such as spherulites. At sufficiently high concentrations (>8 mol % comonomer[32]), crystallization is limited to neighboring ethylene sequences resulting in bundle-like crystals often termed fringed micelles. All of these observations are the result of the exclusion of short-chain branches from the crystal when the branches are longer than a methyl group (methyl groups are incorporated into the crystal lattice to a substantial degree resulting in distorted unit cells[33, 34, 39-42]). Similar behavior has been observed between HPBD and LCB-free metallocene copolymers, which have been studied containing ethyl, butyl, and octyl branches.[43, 44] Accordingly, in most cases the branch length was found to be irrelevant since their primary role is as defects.[34, 39, 41, 45, 46] Some authors argue that ethyl branches are incorporated into the crystal to a small degree,[47-49] however, this effect must be minor since evidence of this is not always observed. The consequence of the exclusion of chain defects is that crystallization is governed by the ethylene sequence length distribution (ESLD) between these short-chain branches. The ESLD dictates the availability of ethylene units having sufficient length to crystallize at a given temperature and is more important than copolymer composition.[34, 46, 50, 51]

Due to the dependence on ESLD, random copolymers exhibit several behaviors that distinguish them from homopolymers. In contrast to homopolymers, the morphology and thermal properties of copolymers are fairly insensitive to crystallization conditions.[43, 52] Furthermore, this sensitivity decreases with increasing SCB content.[30, 53] As discussed below, in contrast to homopolymers, crystallization kinetics of copolymers appears to be only weakly dependent on melt dynamics. Additionally, there is on-going debate about the evolution of morphology during crystallization due to the unusual observation of dual melting endotherms by Differential Scanning Calorimetry (DSC) following isothermal crystallization.

Initial theories to account for this double melting behavior of copolymers centered on the melting-recrystallization-remelting (mrr) phenomenon that is commonly observed in thin homopolymer crystals.[54] However, careful DSC studies have indicated that the distinct double melting behavior (e.g., Figure 3.5) is not the result of mrr.[21, 34, 43, 45, 55-59] While mrr has been confirmed for copolymers with a small amount of short-chain branching, the phenomenon is manifested as an additional third peak that is much smaller in magnitude and only observed at low heating rates.[60, 61] Presently, double melting is commonly attributed to two crystal populations having different thermal stabilities.

A number of theories have been presented to account for the differences in thermal stability of crystals supposedly formed at the same isothermal temperature (T_c). One widespread theory advocates differences in morphology between the two populations: ethylene sequences that are long enough to rapidly chain-fold into lamellae while those that are shorter, but are still capable of crystallization at T_c, crystallize much slower with nearest-neighbor ethylene sequences into fringed micelles. [43, 45, 52, 55, 61] Another theory is

that the two populations contain equal lamellar thicknesses but a bimodal distribution of density and surface characteristics.[62] An alternative explanation is based on a bimodal lamellar thickness distribution: longer ethylene sequences crystallize rapidly forming thick lamellae while thinner, less thermally stable lamellar crystals form slowly from shorter ethylene sequences.

In the present work, we examine double melting behavior and other aspects of crystallization of HPBDs of different molecular architectures (short linear, long linear, star, and H-polymer). We investigate the effect of long-chain branching on thermal and morphological properties in these model systems. Accounting for previous studies, morphology evolution both during temperature ramps and under isothermal conditions is re-evaluated. Finally, we comment on the implications of our findings on the use of these materials as model systems for studying the effects of melt dynamics on flow-induced crystallization.

3.2 EXPERIMENTAL METHODS

3.2.1 Materials

The majority of the materials used in these studies are hydrogenated polybutadienes (HPBDs) that were synthesized via anionic polymerization followed by hydrogenation. This method, in conjunction with hydrosillation, allows for the synthesis of molecules that are well-defined in both long-chain branching (LCB) and molecular weight (PDI = $M_w/M_n < 1.1$).[22, 27] The resulting materials are analogous to random ethylene-co-butenes with a minimum of 7 wt % butene—in other words, 19 or more ethyl side groups per 1000 backbone carbon atoms. HPBD materials were graciously provided by

ExxonMobil in collaboration with Professor Nikos Hadjichristidis (University of Athens, Athens, Greece) and characterized by Dr. David Lohse and his team (ExxonMobil, Clinton, NJ).

Table 3.1 Molecular characteristics of polyethylene materials examined. All values provided by ExxonMobil.

Polymer	Type	$M_{w,tot}$ (kg/mol)	PDI	$M_{w,b}$ (kg/mol)	$M_{w,a}$ (kg/mol)	SCB/ 1000 backbone C[a]
L53	Linear	53	<1.05	53		19.2
L152	Linear	152	<1.05	152		19.5
S3	3-arm star	141	<1.05		47	18.9
H4	H-polymer	156	<1.05	112	11	26.3
HDPE	Linear	529	3.0	529		0.2

[a] obtained via ^{13}C NMR

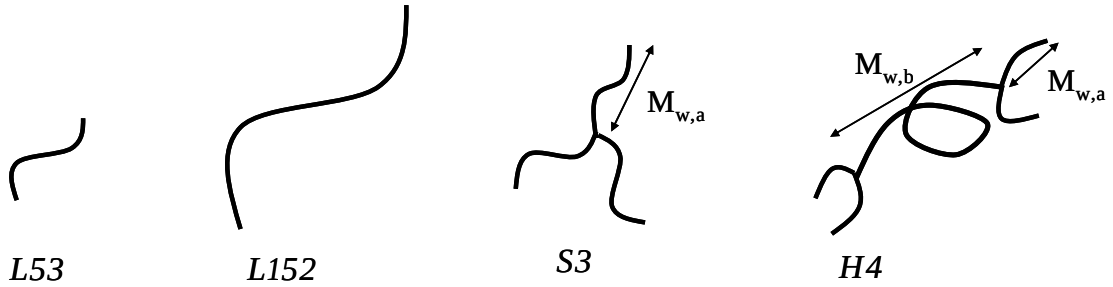

Figure 3.2 Schematic representation of the four HPBD materials examined: short linear (L53), long linear (L152), 3-arm star (S3), and H-polymer (H4).

Quiescent crystallization was studied on four HPBDs (Table 3.1): two linear chains (L53 and L152) and two molecules containing long-chain branches—a symmetric, three-arm star (S3) with each arm having molecular weight ($M_{w,a}$) of 47 kg/mol and an H-polymer (H4) with a backbone molecular weight ($M_{w,b}$) of 112 kg/mol and two 11 kg/mol arms on each end (Figure 3.2). In this context, 'linear' refers to molecules that are free from LCB; as mentioned above, all chains contain short-chain branches (SCB). It is important to note that L53, L152, and S3 all contain approximately 19 branches per

1000 carbon atoms—the minimum SCB content accessible via anionic polymerization. The H4 polymer has higher overall SCB content than the rest, despite having arms with similar SCB content to the previous three samples; the difference originates from the synthetic route to the telechelic backbone, which results in higher SCB content along the backbone. Consequently, the H4 molecule has a homogenous SCB distribution within each long branch but not within each molecule. Additionally, high density polyethylene (HDPE) was included for comparison (no LCB and very few SCB).

Comparison of these molecules enables elucidation of the effects of molecular weight (L53 versus L152) and long-chain branching (L152 versus S3). Effects of short-chain branching are difficult to isolate because the comparison of L152 or S3 to H4 is more complicated due to the combined effects of LCB, overall SCB content, and intramolecular SCB distribution. However, in most cases, SCB effects can be inferred based on prior literature.

3.2.2 Differential Scanning Calorimetry

Differential Scanning Calorimetry (DSC) experiments were conducted by Dr. Soo-Young Park (Kyunpook National University, Daegu, South Korea) to study thermal transitions of each polymer (5-10 mg samples) using a Perkin Elmer 7 DSC system calibrated with an indium standard. Both temperature ramps and isothermal studies were conducted under a nitrogen atmosphere. Peak melting and crystallization temperatures were obtained during cooling and subsequent heating ramps performed at 10 °C/min from 140 to 40 °C. Additional scans at 10 °C/min were conducted by Dr. Manika Varma-Nair (ExxonMobil, Clinton, NJ) in a larger temperature range of 160 to -30 °C.

Isothermal crystallization was conducted at a variety of temperatures for each polymer. After erasing thermal history at an elevated temperature of 130 °C, a 5-10 mg sample was cooled to the desired crystallization temperature, T_c, at 40 °C/min. The sample was left at this temperature for 30 minutes and then heated at 10 °C/min; heat flow was monitored throughout the experiment. Additional isothermal studies were conducted by Robert Panepinto (ExxonMobil, Clinton, NJ) for independent validation using the same isothermal temperatures but a higher temperature (140 °C) to erase thermal history and a faster cooling rate (~200 °C/min) to T_c.

3.2.3 X-ray Scattering

Morphology development during heating and cooling ramps was followed using wide angle and small angle x-ray scattering (WAXS and SAXS, respectively). An INSTEC STC200 hot stage was used to subject samples to temperature ramps at 10 °C/min in a range of 160 to 0 °C. Samples were placed between Kapton tape into a holder with 0.5 cm diameter and 1.558 mm thickness. Additional SAXS experiments, termed 'ramp-iso', included temperature ramps (10 °C/min) with a 30-minute, isothermal step at a temperature approximately 16 °C below T_m (apparent subcooling, $\Delta T = T_m - T_c \approx 16$ °C). There isothermal temperatures were $T_c = 95$ °C for L53, $T_c = 87$ °C for L152 and S3, and $T_c = 76$ °C for H4. For comparison, L53 was also subjected to the same ramp with an isothermal step at 102 °C—the highest isothermal DSC temperature at which two melting peaks were observed.

Scattering experiments were carried out at beamline X27C of the National Synchrotron Light Source (NSLS, Brookhaven National Lab, Upton, NY).[63] A MARCCD

detector with 158 μm pixel size was used to record two-dimensional scattering patterns generated with x-rays having a wavelength, λ, of 1.371 Å. For WAXS experiments, the detector was placed 11.4 cm from the sample and camera length was calibrated using aluminum oxide (Al_2O_3). For SAXS, the sample-to-detector distance was 1.9 m, and calibration was conducted using silver behenate. One scattering image was collected every 2 °C.

SAXS data during temperature ramps for H4 were obtained at beamline 7.3.3 of the Advanced Light Source (ALS, Lawrence Berkeley National Lab, Berkeley, CA).[64] Scattering data was collected using an ADSC Quantum 4u CCD detector at a distance of 2.84 m and a source wavelength, λ, of 1.371 Å. The sample-to-detector distance was calibrated using silver behenate. A Linkam calorimetry stage was used to subject samples pressed in aluminum pans to temperature ramps at 10 °C/min from 160 to 0 °C while measuring heat flow. One scattering image was collected every 7 °C. Data collected at both beamlines for L53 and S3 were compared for consistency.

X-ray data pre-treatment included the subtraction of a background and adjustment for incident x-ray beam flux and acquisition time. The integrated intensity was extracted as a function of scattering vector, $q = 4\pi\sin(\theta)/\lambda$, where θ is the scattering angle. Since the samples were isotropic, a Lorentz correction[65] was applied by multiplying the scattering intensity, $I(q)$, by the square of scattering vector, q: $J(q) = I(q)q^2$.

The SAXS long period, L_p, was determined from the position of the peak in $J(q)$, q_{max}, as: $L_p = 2\pi/q_{max}$. The long period is a measure of the periodicity within the sample resulting from electron density differences and is interpreted as a characteristic spacing of crystalline and non-crystalline domains for a two-phase system. The area under the Lor-

entz-corrected SAXS intensity curve (for isotropic samples) in the full range of q ($0 < q < \infty$) defines the invariant, which is a measure of the total scattering power of the sample. Given the experimental constraints, we approximate the invariant by the integrated intensity, Q, in the range available ($q_{min} < q < q_{max}$):

$$Q = \int_{q_{\min}}^{q_{\max}} q^2 I(q) dq \,. \tag{3.1}$$

The WAXS crystallinity index, X_c, was determined as the ratio of the area of the crystalline peaks, A_c, to the combined area of the amorphous halo, A_a, and the crystalline peaks: $X_c = A_c/(A_a+A_c)$. Areas were obtained after fitting the amorphous halo and the orthorhombic crystal reflections due to the (110)- and (200)-planes with Lorentzian functions using Origin 7.5. X-ray data analysis was conducted using code written in MATLAB R2008b (Thesis Appendix A).

3.3 RESULTS

3.3.1 Differential Scanning Calorimetry

3.3.1.1 Temperature Ramps

Heating and cooling traces for each material are shown in Figure 3.3. In agreement with prior literature, the crystallization exotherms for the HPBD materials contain two peaks: the primary peak at higher temperatures ($T_{x,high}$) and a much smaller peak at lower temperatures ($T_{x,low}$; marked by asterisks in Figure 3.3a).[45, 66] The low crystallization peak is least prominent for H4. Upon subsequent heating, only one broad peak is observed. Nearly identical behavior is observed for L152 and S3. As expected, HPBDs exhibit smaller, broader DSC peaks as a consequence of the ethylene sequence length dis-

tribution.[21, 32, 43, 45, 52, 57, 67]

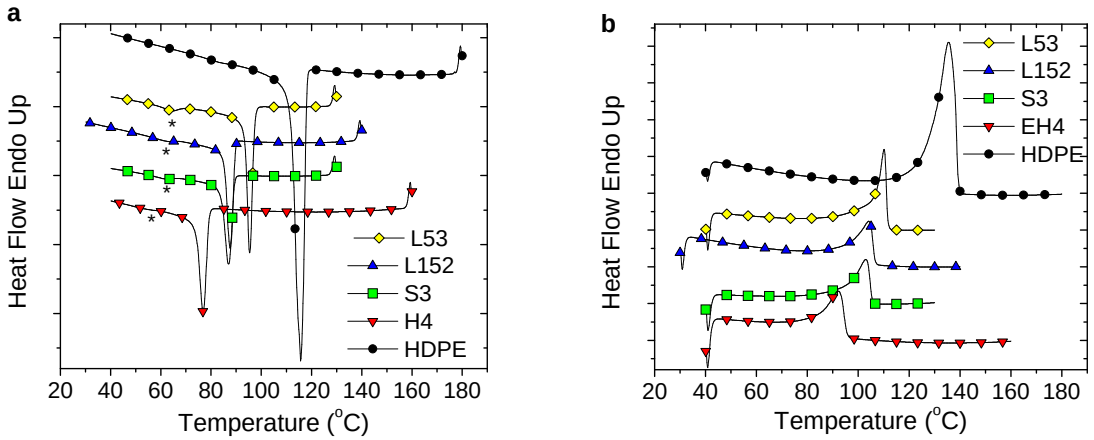

Figure 3.3 DSC **a)** cooling and **b)** heating traces obtained at 10 °C/min. Asterisks mark $T_{x,low}$.

Corresponding peak melting and crystallization temperatures (T_m and T_x, respectively) for each material are tabulated in Table 3.2. All three transition temperatures decrease with both increasing molecular weight (L53 vs. L152) and SCB content (L152 vs. H4), as has been observed previously as a consequence of decreased crystal size. [21, 30, 32, 35, 36, 44, 48, 52] Transition temperatures for L152 and S3 are nearly identical.

Table 3.2 Peak transition temperatures obtained by DSC during heating and cooling ramps at 10 °C/min.

Polymer	$T_{x,low}$ (°C)	$T_{x,high}$ (°C)	T_m(°C)
L53	64.3	95.3	110.2
L152	61.8	87.6	104.4
S3	61.5	87.0	102.9
H4	56.6	76.8	92.2
HDPE		117.7	135.7

3.3.1.2 Isothermal Crystallization

Crystallization kinetics of each material were examined during isothermal crystallization. As done by Haigh et al.,[68] the time necessary to reach 10% of the maximum crystallinity ($t_{0.1}$) at a given temperature was taken as a measure of the crystallization rate.

From Figure 3.4, it is clear that HDPE exhibits the fastest crystallization kinetics, as expected, while H4 exhibits the slowest. In agreement with Haigh et al., L53 has the fastest kinetics out of the HPBDs examined due to its low molecular weight.[35, 68] Differences in crystallization kinetics due to the presence of long-chain branching, expected based on prior literature,[4, 68, 69] were not immediately observed since L152 and S3 exhibited very similar behavior.

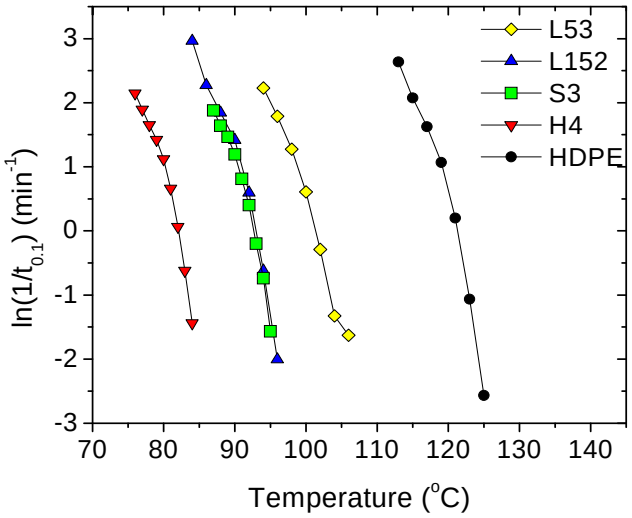

Figure 3.4 Crystallization kinetics represented as the amount of time necessary to reach 10% maximum crystallinity ($t_{0.1}$) as a function of the isothermal crystallization temperature.

Melting traces following isothermal crystallization of HPBD materials are characterized by two peaks, high-melting ($T_{m,high}$) and low-melting ($T_{m,low}$), at all but the highest crystallization temperatures examined.[21, 43, 45, 55, 70] When comparing traces at similar apparent undercoolings, $\Delta T = T_m - T_c$, the magnitude of both peaks appears to be only a function of molecular weight and not SCB content or distribution. As an example, melting traces for each sample isothermally crystallized at ΔT = 16 °C are shown in Figure 3.5. Aside from HDPE, which only exhibits the expected single melting peak, L53 has

the largest high-melting peak. Again L152 and S3 possess nearly identical traces. The melting trace for H4, although shifted to lower temperatures due to increased SCB content, is very similar to the two HPBDs of similar molecular weight. Closer examination, however, reveals a larger low-melting peak for H4 than for L152 and S3.

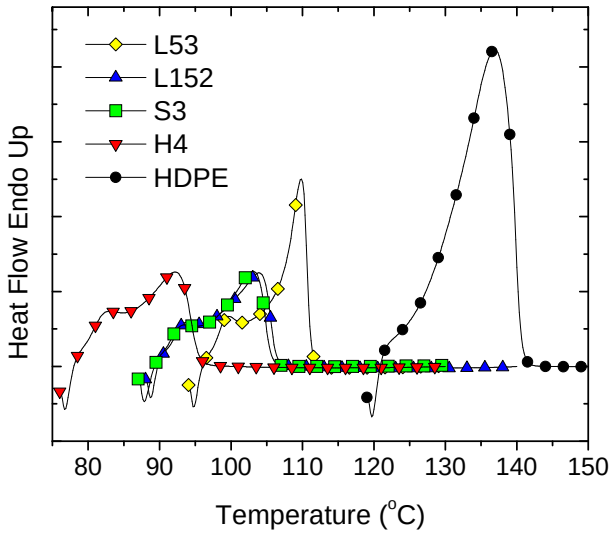

Figure 3.5 DSC melting traces obtained during heating at 10 °C/min following isothermal crystallization for each material at $T_c = T_m - 16$ °C.

An examination of the dependence of both melting peak temperatures on the isothermal crystallization temperature reveals interesting behavior typical of copolymers (Figure 3.6). Plotting melting point as a function of the isothermal crystallization temperature (sometimes called a Hoffman-Weeks plot) is often used to determine the equilibrium melting temperature of a semicrystalline polymer. For homopolymers like HDPE, extrapolating T_m versus T_c to the melting temperature of a perfect crystal (i.e., the intersection of a linear fit through T_m versus T_c with the $T_m = T_c$ line) reveals the equilibrium melting temperature.[71, 72] However, this procedure fails when applied to either melting peak of copolymers.[43, 44, 73] The high-melting peak appears nearly independent of the iso-

thermal crystallization temperature, while the low-melting peak is parallel to $T_m = T_c$.[47, 58, 61, 70]

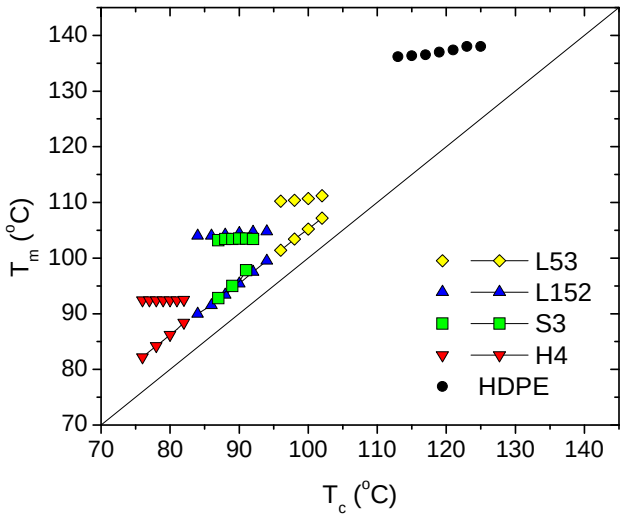

Figure 3.6 Peak high-melting (symbols) and low-melting (line + symbols) temperatures as a function of isothermal crystallization temperature (T_c) obtained during heating in DSC at 10 °C/min.

The average high-melting peak value ($T_{m,high}$) for each material is insensitive to T_c, in agreement with past literature,[43, 70] and is very similar to the peak melting temperature obtained during temperature ramps (Table 3.3 versus Table 3.2).[43] The extent to which $T_{m,high}$ changes with T_c, characterized by the approximate slope of $T_{m,high}$ versus T_c, $\Delta T_{m,high}/\Delta T_c$ (Table 3.3), is greatest for the short linear HPBD and least for the H-polymer.

Table 3.3 Average high-melting peak ($T_{m,high}$) obtained during heating at 10 °C/min subsequent to isothermal crystallization and its dependence on the change in the isothermal crystallization temperature.

Sample	$T_{m,high}$ (°C)	$\Delta T_{m,high}/\Delta T_c$
L53	110.5 ± 0.5	0.23
L152	104.4 ± 0.4	0.08
S3	103.4 ± 0.1	0.06
H4	92.4 ± 0.1	0.02

The low-melting peak ($T_{m,low}$) appears to be offset from the isothermal crystallization temperature by a constant (Figure 3.6).[43, 55, 59, 60, 74] This constant appears to be independent of not only SCB content and molecular weight, as demonstrated by Alamo et al.,[44] but also long-chain branching.

3.3.2 X-ray Scattering

3.3.2.1 WAXS: Temperature Ramps

A comparison of the temperature dependence of the WAXS crystallinity, X_c, during temperature ramps revealed a strong dependence on SCB content (Figure 3.7).[29, 30, 33-35] Additionally, two types of behavior were observed: (1) the expected hysteresis in crystallinity during cooling and heating at elevated temperatures termed 'irreversible' crystallization and melting because crystals formed during cooling required higher temperatures to melt and (2) 'reversible' crystallization and melting at lower temperatures where crystallinity values during cooling and subsequent heating overlap. These two regimes are consistent with previous DSC, SAXS, and WAXS studies on polyethylenes containing short-chain branches.[45, 62, 66, 67, 75, 76]

The presence of short-chain branching in L152 results in a decreased transition temperature between reversible and irreversible behavior, $T_{r,w}$ (defined as the temperature at which crystallinity upon cooling and subsequent heating differs by less than 10%), compared to HDPE (Figure 3.7). A small amount of reversible crystallization of HDPE (~15%), occurring between $T_{r,w}$ and 0 °C, is attributed to surface crystallization/melting.[75, 77] In contrast, reversible crystallization accounts for a greater percentage of total crystallinity at 0 °C in L152 (~25%). Additionally, irreversible crystallization and

melting of L152 occurs over a larger temperature range than HDPE because it is governed by the ESLD.[50, 78] Of added interest is the lull in crystallinity evolution apparent at temperatures immediately above $T_{r,w}$ in all HPBD materials examined (marked by an asterisks in Figure 3.7). Possible explanations for this observation are detailed in the discussion section.

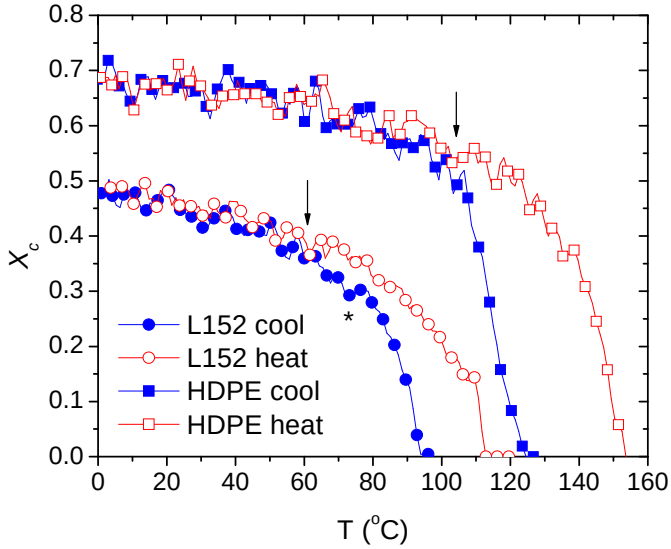

Figure 3.7 Crystallinity determined by WAXS as a function of temperature during heating and cooling ramps of L152 and HPDE at 10 °C/min. Arrows indicate $T_{r,w}$. Asterisk marks lull in crystallinity evolution.

A comparison between the four HPBD materials reveals that $T_{r,w}$ is greatest for L53 (71 ± 3 °C) and is within the range of 62.8 ± 3.8 °C for the higher molecular weight HPBDs, with S3 being at the high end of the range (Figure 3.8, open triangles). The similarity of $T_{r,w}$ between L152 and H4 is inconsistent with previous observations of the transition temperature decreasing with increasing SCB content.[45] The corresponding crystallinity at $T_{r,w}$, $X_c(T_{r,w})$, is similar for the three materials of similar SCB content (L53, L152, and S3) at 39 ± 4% (Figure 3.8, filled squares). As expected, H4 exhibits lower crystallin-

ity (31 ± 3%) due to its increased SCB content.[29, 30, 33, 34] A similar trend is observed at T = 0 °C (X_c(0 °C) in Figure 3.8, filled circles). The slightly elevated crystallinity of S3 compared to L152 at 0 °C can be attributed to the small difference in SCB content between the two materials (18.9 for S3 versus 19.5 for L152; Table 3.1) and further highlights the significance of short-chain branching. The relative amount of reversible crystallization appears to be in the same range for all four materials, with S3 again being at the high end of the range (difference between filled circles and squares in Figure 3.8). This observation is inconsistent with previous works that found that the relative amount of reversible crystallization increases with increasing SCB content.[45, 75, 79]

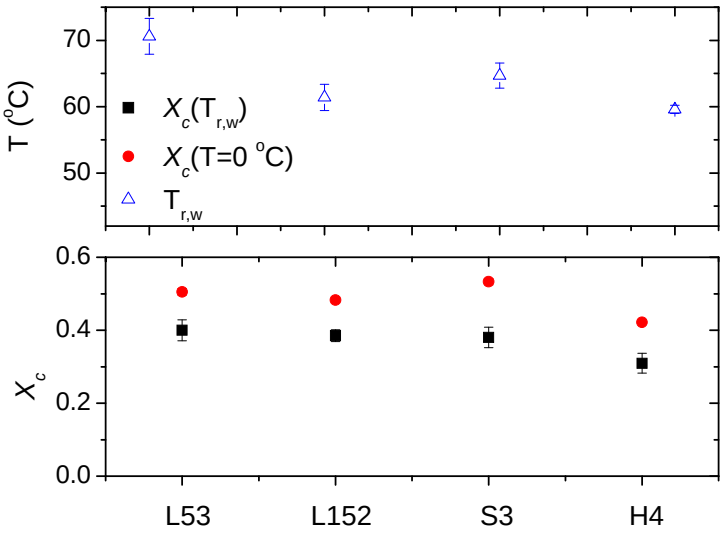

Figure 3.8 WAXS-determined transition temperature ($T_{r,w}$) to reversible crystallization, the crystallinity at that temperature ($X_c(T_{r,w})$), and the maximum crystallinity obtained (X_c(0 °C)) for each HPBD material.

3.3.2.2 SAXS: Temperature Ramps

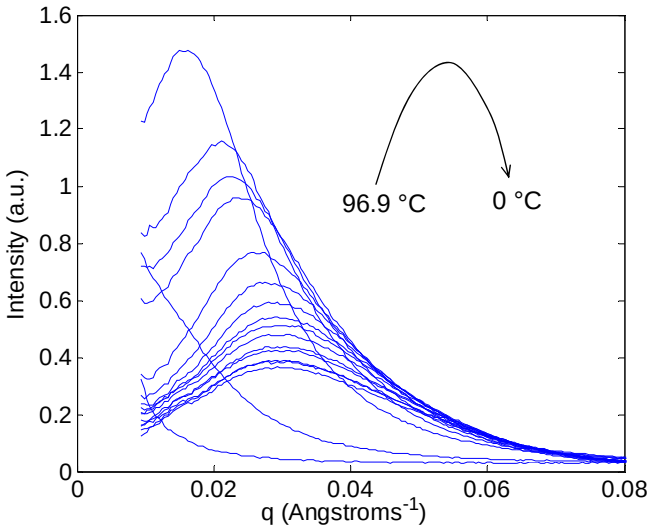

Figure 3.9 SAXS intensity collected during cooling of L152 at 10 °C/min (1 trace every ~6 °C). Arrow shows general peak movement in temperature range examined.

SAXS scattering curves exhibited significant variation in peak height, width, and position with temperature (e.g., Figure 3.9), as seen in previous investigations of polyethylenes containing short-chain branching.[66, 80-83] An example of the general trend is exhibited by L152 during a cooling ramp. Initially, SAXS intensity, $I(q)$, grows at low q-values, corresponding to zero scattering angle, similar to HDPE;[84, 85] then a peak develops and grows in intensity while its position moves to higher q-values; eventually, it reaches a maximum and declines while broadening and moving further to higher values of q. At lower temperatures, the peak position reaches a plateau at $q \sim 0.033$ Å^{-1} but continues to broaden at the expense of peak height.

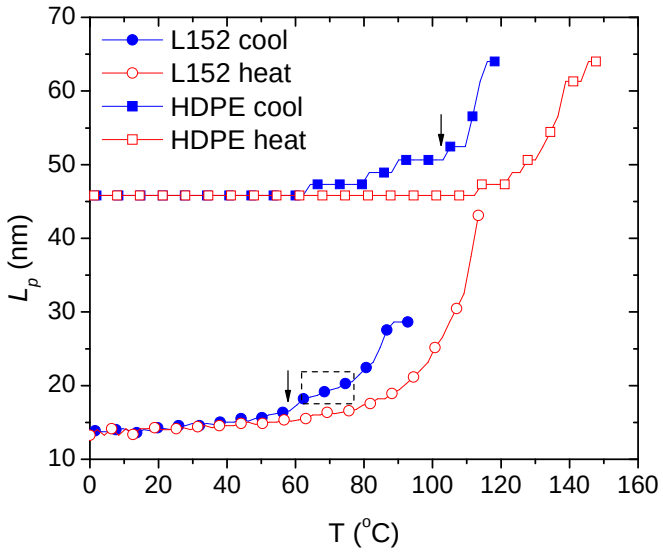

Figure 3.10 Long period as a function of temperature during heating and cooling ramps of L152 and HPDE at 10 °C/min. Box identifies lull in long period evolution. Arrows mark $T_{r,s}$.

The long period, L_p, determined by SAXS of all materials examined exhibited regions corresponding to reversible and irreversible crystallization (Figure 3.10), similar to crystallinity evolution (Figure 3.7).[67, 80] However, during reversible crystallization, the long period of HDPE remains constant while that of HPBD materials continues to decrease, as has been observed previously.[48, 79, 80, 83, 86-88] Below the transition temperature, $T_{r,s}$ (defined as the temperature at which the difference in long period during cooling and subsequent heating is less than 10%), the HDPE long period varies less than 2%. In contrast, the long period of L53 decreases by 8%, that of L152 and S3 by 14%, and that of H4 by 23%. The transition temperature itself follows a similar trend: largest for L53, lowest for H4, and of similar intermediate values for L152 and S3 (Figure 3.11, open triangles). Consequently, $T_{r,s}$ and the amount of change in L_p during reversible crystallization appear to be a function of molecular weight and SCB content, but not long chain

branching.

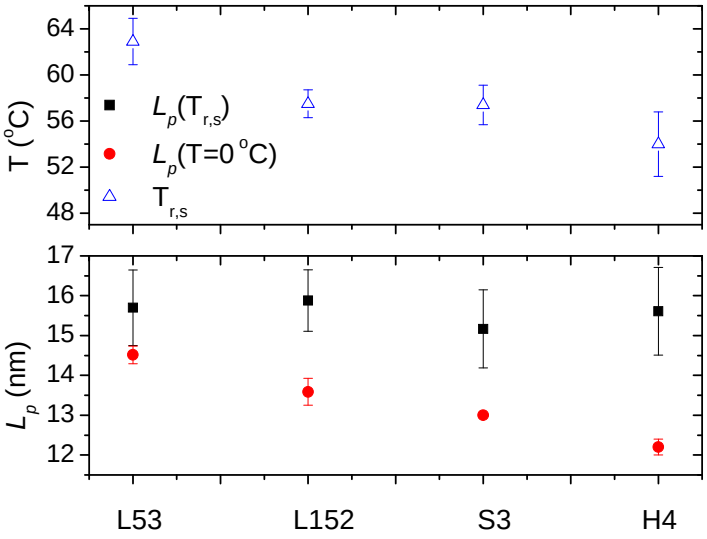

Figure 3.11 SAXS-determined transition temperature ($T_{r,s}$) to reversible crystallization, the long period at that temperature ($L_p(T_{r,s})$), and the minimum long period obtained (L_p(0 °C)) for each HPBD material.

All HPBD materials exhibit a similar long period at $T_{r,s}$, $L_p(T_{r,s})$, of 15.5 ± 1 nm (Figure 3.11, filled squares). In contrast, the long period at T = 0 °C, L_p(0 °C), appears to be dependent on molecular weight, short-chain and long-chain branching with L53 > L152 > S3 > H4. The variation among the first 3 materials is inconsistent with the work of Alamo et al. who observed similar room-temperature long periods for samples of similar SCB content but different molecular weight.[44]

All four HPBD materials examined exhibited a lull in the evolution of long period during crystallization, which is highlighted in Figure 3.10. When observed in a previous study, this inflection in L_p versus T was attributed to the transition of the system to a homogenous crystallinity distribution.[66] In agreement with this previous study, the increased change in long period at temperatures immediately below this lull is near the low crystal-

lization temperature observed by DSC ($T_{x,low}$; Figure 3.3 and Table 3.2). Furthermore, this inflection point coincides with the maximum in the SAXS integrated intensity (Figure 3.12), which also exhibits reversible and irreversible crystallization/melting.

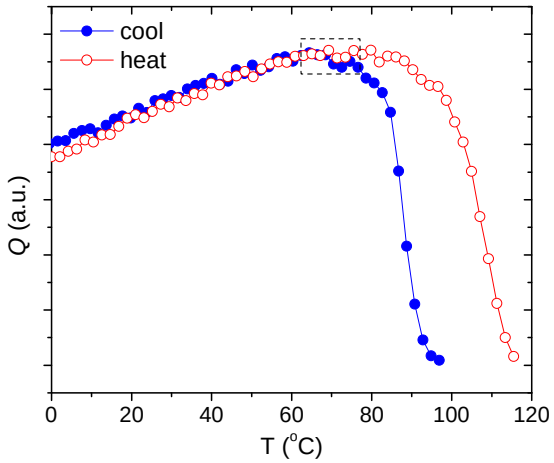

Figure 3.12 SAXS integrated intensity during cooling and heating of L152 at 10 °C/min. Box identifies region corresponding to lull in long period evolution (Figure 3.10).

A final observation of interest is the difference in transition temperatures between irreversible and reversible behavior as determined by WAXS crystallinity, SAXS integrated intensity, and long period. The transition temperature to reversible integrated intensity behavior is the highest of the three and occurs near the maximum of the scattering power during cooling. The temperature to reversible crystallinity evolution is higher than that of long period evolution indicating that there is a small window upon cooling and heating during which the formation of reversible crystals leads to irreversible changes in long period.

3.3.2.3 SAXS: Temperature Ramps with Isothermal Step

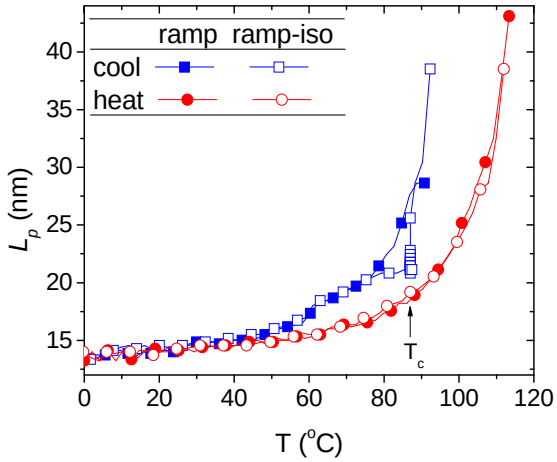

Figure 3.13 Evolution of SAXS long period for L152 during temperature ramps at 10 °C/min (filled symbols) and the ramp-iso protocol with an isothermal step at T_c = 87 °C during cooling (open symbols).

Further insight into the crystallization behavior of these materials may be gained by inserting an isothermal step during cooling ("ramp-iso" protocol). During the hold at T_c, the long period decreased to a limiting value (e.g., L152 in Figure 3.13). For L152, L_p decreased from approximately 26 to 21 nm during the 30 minute hold at 87 °C. Once cooling was resumed, a short induction period was observed before the long period continued to decrease; the evolution of L_p during further cooling coincided with that observed in a continuous ramp (compare filled and open squares for T < 75 °C in Figure 3.13). Long period evolution during subsequent heating traces was very similar for both protocols (open vs. filled circles in Figure 3.13), in agreement with previous works indicating minimal effects of thermal and mechanical history on random copolymers.[52,62,86,89] A reversible crystallization region was still observed. Similar behavior as depicted above was observed for the other HPBDs.

During the 30-minute isothermal hold at similar apparent subcooling $\Delta T = T_m - T_c = 16$ °C, L152 unexpectedly developed a long period that was larger by almost 1 nm compared with L53 and S3 (Figure 3.14). The long period obtained for S3 was only slightly smaller than that of L53. Due to its high nominal melting point, L53 was anticipated to develop morphology with the largest characteristic length scale out of the trio.

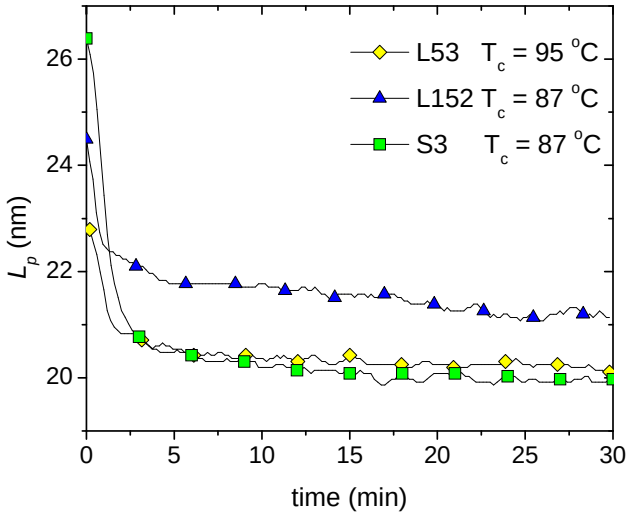

Figure 3.14 Long period of HPBD materials as a function of time during isothermal crystallization at $T_c = T_m - 16$ °C inserted into a cooling ramp at 10 °C/min.

Further insight into evolution of morphology can be gained through the examination of scattering patterns corresponding to the first two minutes of the isothermal step (Figure 3.15). No noticeable crystallization occurred during cooling to a lower ΔT (L53 at 102 °C, Figure 3.15a); during the first two minutes, SAXS intensity increased while peak position only shifted slightly, consistent with isothermal growth dominated by a single long spacing. Upon reaching $\Delta T \sim 16$ °C, each material already possessed a well-defined long period (Figure 3.15b, c, and d). For L53 and S3, scattering intensity initially increased at all *q*-values. L53 exhibited growth in peak intensity in conjunction with mild

peak position shifting until crystallization slowed significantly (evidenced by highly overlapped scattering curves in Figure 3.15b). In contrast to S3 and L152, L53 did not exhibit any obvious decrease of SAXS intensity during isothermal treatment.

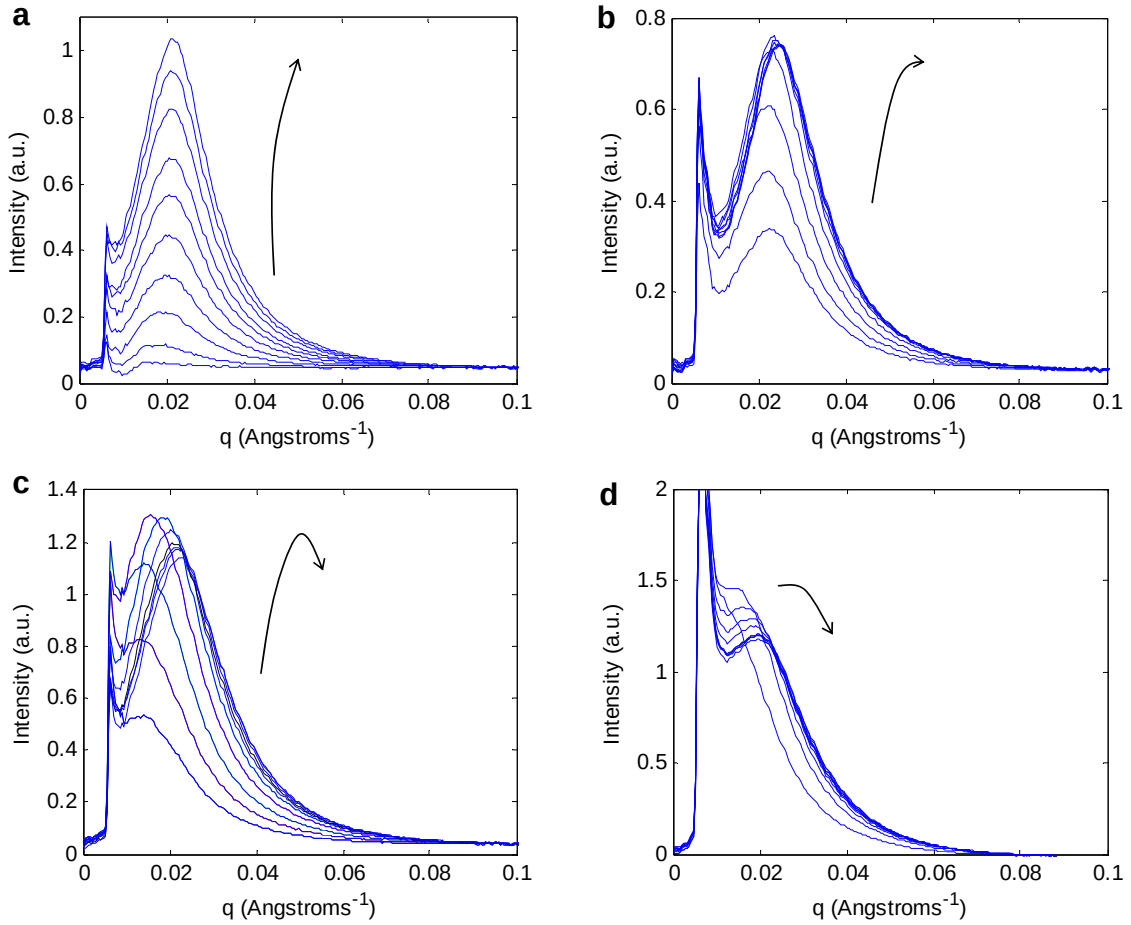

Figure 3.15 SAXS intensity during the first 120 s of isothermal crystallization (1 trace every 12 s): **a)** L53 at 102 °C, **b)** L53 at 95 °C, **c)** S3 at 87 °C, and **d)** L152 at 87 °C. Arrows indicate trend in peak movement.

S3 exhibits a SAXS peak in Figure 3.15c that initially starts at a smaller q-value compared to L53 (corresponding to a larger L_p). This peak shifts gradually to larger q-values while intensity first grows and then decreases before the crystallization rate slows. Decreasing SAXS intensity is consistent with the elimination of the corresponding long periods via lamellar insertion. This process is more prevalent for S3 than L53 given that

S3 was crystallized at a lower temperature, providing adequate driving force for crystallization of shorter ethylene sequences.

L152 exhibited strikingly different behavior: scattering intensities at low q-values decreased after only 12 s of isothermal crystallization. Compared with S3 and L53, L152 underwent little isothermal crystallization, indicating that most of the crystallization occurred during cooling. Hence, the predominant long period was larger due to its formation at higher temperatures—relative to the nominal melting point—compared to S3 and L53.

The pronounced difference in behavior between S3 and L152 is very surprising given the similarity in DSC results. Upon closer inspection, the slight difference in crystallization kinetics at $T_c = 87$ °C between L152 and S3 (Figure 3.4) corresponds to approximately 10% faster crystallization of L152 compared with S3. This relatively small difference in crystallization kinetics has significant impact on morphology development because of the limited amount of copolymer that is able to crystallize at elevated temperatures. Hence, the faster-crystallizing L152 completes most of its primary lamellar growth before reaching $T_c = 87$ °C.

3.4 DISCUSSION

3.4.1 Morphology Evolution during Cooling and Heating

Similar to homopolymers, copolymers require supercooling of the melt to achieve crystallization. Nucleation and growth is responsible for the irreversible behavior observed at higher temperatures both in WAXS crystallinity (X_c; Figure 3.7, $T > T_{r,w}$), SAXS long period (L_p; Figure 3.10, $T > T_{r,s}$) and SAXS integrated intensity (Q; Figure

3.12). The irreversible crystallization/melting region of random copolymers includes two qualitatively distinct subdivisions that can be seen by comparing Figure 3.7, Figure 3.10 and Figure 3.12, as is done in Figure 3.16a. The irreversible regime includes an upper-temperature window in which the three morphological quantities, X_c, L_p, and Q, show a pronounced hysteresis as well as a lower-temperature window in which hysteresis effects are milder. Based on the dominant morphological features that form in each regime (see below), we term the former 'primary-irreversible' crystallization/melting and the latter 'secondary-irreversible' crystallization/melting. The lowest temperature range defines the 'reversible' crystallization/melting regime, in which the three morphological quantities exhibit distinctly similar values upon cooling and heating.

3.4.1.1 Primary-Irreversible Crystallization

During cooling, the onset of crystallization in the polymer system is followed by relatively fast crystallization that is associated with the largest changes in morphology. The corresponding formation of the primary DSC exotherm ($T_{x,high}$ in Figure 3.3) indicates that a large fraction of the total crystallization occurs by nucleation and growth in this primary-irreversible regime.[67] We envision this occurring by the propagation of primary lamellae through an unconstrained melt (Figure 3.16b), in agreement with previous theories.[45, 55] During cooling through the primary-irreversible regime, lamellae form with continuously decreasing long periods resulting in a shift in the SAXS peak to high wavevectors. This behavior is partially a consequence of kinetic effects but primarily due to the limit on the amount of crystallizable material at each temperature based on the ethylene sequence length distribution (ESLD).

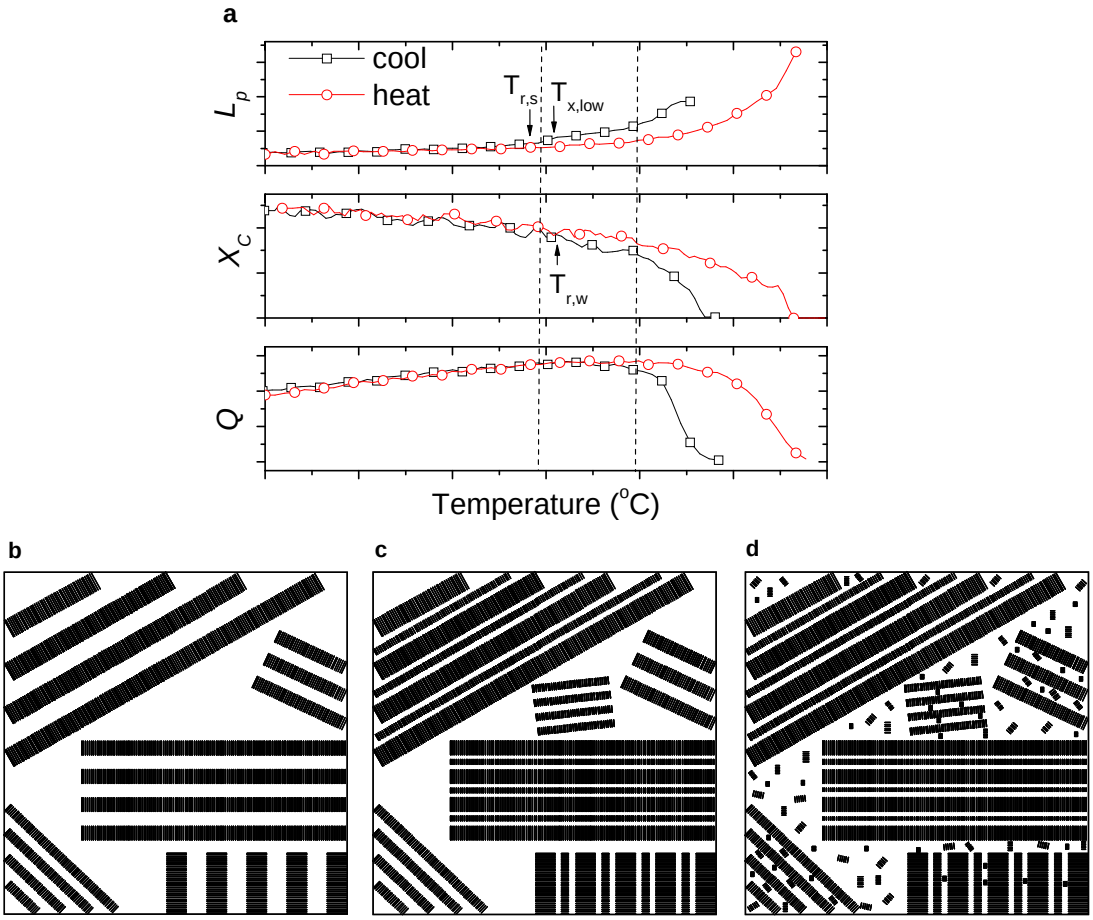

Figure 3.16 a) General representation of SAXS long period (L_p), WAXS crystallinity (X_c), and SAXS integrated intensity (Q) during cooling and subsequent heating ramps defining three crystallization regimes of random copolymers ($T_{r,w}$, $T_{r,s}$, and $T_{x,low}$ are marked for reference). Schematic representation of morphology in each regime: **b)** primary-irreversible at high-temperatures, **c)** secondary-irreversible, and **d)** reversible crystallization at low temperatures.

Due to the ESLD, the long period of random copolymers during irreversible crystallization is dictated by the size of the non-crystalline layers. Previous studies have demonstrated that the crystalline layer thickness is unaffected by temperature,[48, 79, 88, 90] and this observation is confirmed by estimates of crystalline and non-crystalline layer thicknesses provided in the Appendix. At the relatively high temperatures in the primary irreversible regime, only a small number of ethylene sequences will be of sufficient length to crystallize. However, due to the homogenous SCB distribution, these sequences have

equal probability of being found in all HPBD chains. Therefore, the incorporation of a small portion of almost all chains results in large non-crystalline layers between primary lamellae formed at the highest temperatures. At lower temperatures in the still high-temperature primary-irreversible regime, a greater number of ethylene sequences become capable of crystallization, resulting in a smaller part of the chain being left entirely out of the crystal corresponding to thinner non-crystalline layers. Therefore, L_p decreases with temperature.

3.4.1.2 Secondary-Irreversible Crystallization

During cooling through intermediate temperatures between the regime of rapid, irreversible crystallization/melting (primary-irreversible regime) and reversible crystallization/melting, X_c and L_p are less dependent on temperature compared with the primary-irreversible regime, consistent with decreased crystallization kinetics. We propose that this slowing of crystallization is a consequence of the depletion of the unconstrained melt (i.e., unpinned chains). Crystallization continues at a slower rate due to decreased chain mobility due to the majority of chains being pinned to already-formed crystals.[45, 66] This pinning severely hinders large conformational changes necessary for chain-folding. However, since crystals formed in this regime continue to exhibit hysteresis between cooling and subsequent heating, nucleation and growth is still expected to be the dominant means of crystallization. Hence, we propose that morphology evolution in this region continues by the growth of lamellae from shorter ethylene sequences that are capable of crystallization at the given temperature. These lamellae will have decreased lateral dimensions and include more defects that those formed during the primary-irreversible regime.[80, 82]

A small fraction of crystallization in this regime occurs in amorphous 'lakes' between primary lamellar stacks that were not able to sustain crystals at larger temperatures.[91] However, examination of the SAXS integrated intensity (Q), which remains nearly constant at its maximum value in this regime, provides further insight about the predominant location of secondary lamellar growth. For an ideal two-phase system, the integrated intensity is proportional to the electron density difference between the two phases ($\Delta\rho = \rho_c - \rho_a$) and the volume fraction of each phase (φ_1 and $\varphi_2 = 1 - \varphi_1$):

$$Q \propto (\Delta\rho)^2 \varphi_1 \varphi_2 . \tag{3.2}$$

Therefore, for a constant electron density difference, Q will exhibit a maximum at 50% crystallinity. However, since crystallinity values in this temperature range are 25% to 35%, a maximum in integrated intensity can be accounted for by a decrease in the electron density contrast that counters the increase in crystallinity.[67] This can be realized via the formation of secondary lamellae between primary lamellae having the largest non-crystalline layers (Figure 3.16c). Consequently, the secondary-irreversible regime is not present in systems like HDPE that do not form large non-crystalline layers that can accommodate secondary lamellar 'in-filling'.

The onset of the intermediate temperature region is marked by a well-defined lull in X_c at approximately 75 °C for L152 in Figure 3.7. Similar observations have been made in other studies, and left unexplained;[66, 67] however, these lulls are not abundant in the literature on copolymer crystallinity evolution. In S3, for example, this lull was almost entirely masked by the uncertainty in X_c, raising the question of whether or not this feature is real.

A possible explanation for these lulls is that they are artifacts of improper fitting

of the WAXS intensity curves. A number of previous studies have noted that fitting the amorphous halo with two peaks, rather than one as was done in this work, yields a better fit and more reasonable behavior of all peaks considered (position, width, etc.).[33, 92-96] Sajkiewicz et al.[92] also observed a lull in the crystallinity evolution upon cooling of linear low density polyethylenes (LDPEs). These authors advocated the use of a three-phase model to account for the presence of a phase having intermediate properties to those of the crystalline and amorphous layers; although this resulted in a better fit and more reasonable behavior of the amorphous halo, the lull in the evolution of crystallinity remained. Hence, we conclude that the lull observed here is not an artifact of an improper fit to the WAXS features.

Based on their theory of the existence of an 'intermediate phase', Sajkiewicz et al. attributed the lull in crystallinity evolution to reorganization of the intermediate and crystalline phases.[92] Although this is a plausible explanation, arguments have been put forth that contribution to the scattering pattern from an intermediate region that is distributed between the crystalline and amorphous phases should be uniform and not limited to a particular angular region.[33, 93] This controversy is further examined in the following chapter using two-dimensional correlation analysis. Without concrete evidence for the existence of an intermediate phase, we attribute the lull to an induction period, which accounts for the temperature difference between the consumption of the unconstrained melt by propagating lamellae and the onset secondary crystallization can occur in constrained melt.

3.4.1.3 Reversible Crystallization at Low Temperatures

At lower temperatures, X_c, L_p, and Q exhibit dynamic yet distinctly similar behavior upon cooling and subsequent heating. A small amount of reversible crystallization of

HDPE (15% of total) occurs at a constant long period and is accounted for by surface crystallization/melting.[75, 77, 97] In contrast, HPBD materials exhibit changes in crystallinity during the reversible step accounting for 20% to 30% of the total at T = 0 °C with corresponding long period changes of 8% to 23%. For copolymers, reversible crystallization and melting can be attributed to very small crystals that form and melt at similar temperatures.[76] This lack of hysteresis suggests a crystallization mechanism dominated by clustering of neighboring ethylene sequences that are capable of crystallization at a given temperature.[67] These ethylene sequences are quite short and bundle into small, imperfect crystals, which are termed fringed micelles. To avoid ambiguity, in this work we define a fringed micelle as a bundle of non-folded chains with some crystallographic order and lateral dimensions that are on the same order of magnitude as the thickness ($d \sim l$; Figure 3.17). These structures are distinct from lamellae, even poorly formed ones, which have thicknesses that are much smaller than their lateral dimensions ($d << l$).

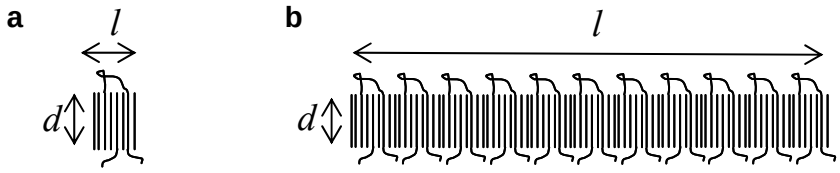

Figure 3.17 Schematic representation of **a)** fringed micelle and **b)** lamellae.

This fringed micelle morphology is consistent with the observations of Alizadeh et al., who found DSC crystallinity to be independent of cooling rate in the reversible regime.[45] This result suggests that crystallization kinetics are not dependent upon the degree of subcooling and is in agreement with fringed micelle formation that is the result of local conformational fluctuations. These fringed micelles form between pre-existing lamellae as evidenced by decreasing SAXS intensity at all q-values during reversible crys-

tallization while crystallinity is below 50% (Figure 3.12).

3.4.1.4 Transition Temperatures

For the HPBD materials, the transition to reversible behavior of the SAXS integrated intensity, Q, occurs near its maximum value. At this temperature, Q becomes dominated by the electron density contrast in the system and not crystallinity, since crystallinity values are still below 50% (see eq 3.2). This temperature is also very close to the transition between the primary-irreversible and secondary-irreversible crystallization regimes, providing further evidence for 'in-filling' of primary lamellae via secondary lamellar growth occurring during secondary-irreversible crystallization.

Furthermore, the transition temperatures to reversible behavior of crystallinity and long period are separated by 4 – 8 °C. At an intermediate temperature, T_1, such that $T_{r,s} < T_1 < T_{r,w}$, the system exists with the same crystallinity during heating as during cooling. However, upon heating, the long period at T_1 is smaller than during cooling. A possible explanation for this observation is if the crystals that melted upon reheating to T_1 are located in different locations than those that formed during cooling below T_1. The implication then is that some crystals formed at lower temperatures turn out to be more stable than those formed at higher temperatures. These more stable crystals are located further away from pre-existing crystal structures, as deduced from their noticeable effect on long period, changes in which are believed to be dominated by changes in the amorphous layer thickness (see Appendix).[80] Upon heating, less stable crystals near crystal surfaces melt, suppressing the expected increase in the long period. This explanation is consistent with the observation that the smallest difference between $T_{r,s}$ and $T_{r,w}$ is exhib-

ited by the H4 polymer, which has a limited number of ethylene sequences of sufficient length to form crystals having increased stability during reversible crystallization.

3.4.2 DSC Double Melting

The evolution of morphology during temperature ramps described above can be reconciled with morphology formation during isothermal crystallization and account for the two DSC melting endotherms (Figure 3.5). We propose that the high-melting peak ($T_{m,high}$) is due to primary lamellae that form from the longest ethylene sequences in unconstrained melt both during cooling to and at the isothermal temperature (T_c). Evidence for crystallization during cooling is demonstrated by the appearance of a SAXS peak immediately upon reaching T_c (Figure 3.15). Additionally, the temperature of the high-melting peak ($T_{m,high}$) following isothermal crystallization and the peak melting temperature (T_m) following a cooling ramp are nearly identical, as previously observed.[43] Furthermore, our observation that $T_{m,high}$ is nearly independent of T_c is supplemented by observations in prior literature showing that $T_{m,high}$ is also independent of crystallization time (t_c).[45, 58, 70] These observations indicate that the high melting fraction is primarily formed during cooling and thus is unaffected by isothermal treatment, as previously suggested by others.[45, 70]

On the other hand, monotonically increasing scattering intensity observed during the first two minutes of isothermal crystallization of L53 and S3 (Figure 3.15a-c) indicates a continuation of the crystallization occurring during cooling, resulting in a fraction of primary lamellar formation at T_c. These lamellae melt at temperatures dependent upon their formation temperature (i.e., T_c) and affect the dependence of $T_{m,high}$ on T_c when

enough lamellae are present. In most cases, as evident from the nearly constant $T_{m,high}$ with T_c (Figure 3.6 and Table 3.3), the portion of primary lamellae formed at T_c is low relative to the amount formed during cooling. However, some samples, like L53, exhibit homopolymer-like behavior manifested in a noticeable slope of $T_{m,high}$ versus T_c (Figure 3.6 and Table 3.3).[45] For these materials, a significant fraction of primary lamellae within the system formed at T_c rather than during cooling. Molecules having lower molecular weight and SCB content are able to crystallize at higher temperatures, at which greater chain mobility and decreased nucleation rates result in less pinning of chains to crystal surfaces; consequently, more unconstrained melt is available for propagation of primary lamellae at the relatively high isothermal temperatures used for these materials. It follows that copolymer effects on thermal behavior are gradual, with greatest homopolymer-like behavior observed in systems with low SCB content and at high temperatures.[45]

The low melting peak ($T_{m,low}$) is universally attributed to species formed at the isothermal crystallization temperature, as is evidenced by the lack of $T_{m,low}$ after short times at T_c.[56] However, there is some speculation as to the morphology of these structures and, hence, the reason behind their decreased thermal stability. We attribute the low-melting peak ($T_{m,low}$) to secondary lamellae that form isothermally from ethylene sequences whose lengths are dictated by T_c. It follows that the thickness of these crystals, and hence, their melting temperature, also depends on T_c. In agreement with Rabiej et al.,[62] but in contrast to other work,[43, 45, 52, 55, 61] we do not use the term fringed micelles to describe these structures since $T_c = T_m - 16$ °C is in the primary-irreversible crystallization regime where fringed micelle formation is not expected. Secondary lamellar growth,

although unexpected, occurs because isothermal treatment provides sufficient time to overcome its sluggish kinetics.

The manifestation of these secondary lamellae is seen in Figure 3.15 as a decrease in scattering intensity at low *q* corresponding to the elimination of the largest long periods. This observation indicates that these secondary lamellae form between pre-existing primary lamellae having the largest non-crystalline regions.[98, 99] This 'in-filling' is most pronounced for L152 and S3 (Figure 3.15c and d). Based on DSC results (not shown), approximately 10% and 17% of total crystallinity at the end of 30 minutes at T_c = 87 °C is attributed to secondary lamellae for L152 and S3, respectively. This significant percentage of secondary crystal growth can be accommodated by the relatively large non-crystalline layers found between lamellae in random copolymers (see Appendix).[48, 79, 80, 88, 90]

Previous literature regarding the increase of $T_{m,low}$ with increasing time at T_c (i.e., offset of the low melting peaks from $T_m = T_c$ in Figure 3.6) has attributed the effect to crystal thickening,[58, 100] decreased conformational entropy of the amorphous phase due to secondary crystallization,[45] or an instrumental artifact.[62] Instead, we propose that sluggish secondary crystallization of short ethylene sequences can result in crystals having progressively greater stability when given more time for close-neighbor ethylene sequences to reorganize.

3.4.3 Effects of Molecular Characteristics

The four HPBD materials were selected in order to evaluate the effects of molecular topology: molecular weight, short-chain and long-chain branching. Comparisons

between L53 and L152 enable the isolation of molecular weight effects. Insight into long chain branching is gained by examining L152 and S3 and effects of short-chain branching can be inferred from L152, S3, and H4. It was found that SCB content and molecular weight has the greatest influence on morphology and crystallization kinetics.

3.4.3.1 Crystallinity

The transition temperature to reversible crystallization, $T_{r,w}$, upon cooling can be interpreted as the temperature at which the long ethylene sequences capable of nucleation and growth of primary and secondary lamellae have been consumed, and only shorter sequences capable of fringed micelle formation remain. Hence, the crystallinity at $T_{r,w}$ decreases with the amount of long ethylene sequences in the molecule and, consequently, with increasing SCB content. In agreement, H4, having the highest SCB content, exhibits the lowest crystallinity at $T_{r,w}$ out of the four HPBD materials examined.

The values for $T_{r,w}$ vary from 32 to 43 °C below the peak melting point determined by DSC, T_m, and speak to the difficultly in defining similar apparent subcoolings ($\Delta T = T_m - T_c$) for the different samples. $T_{r,w}$ appears to be dependent primarily on molecular weight, which determines the amount of pinning of chains during crystallization. For example, at the same temperature, L152, which has three times the molecular weight of L53, contains three times as many crystallizable ethylene sequences, and hence three times as many pinning cites, resulting in greater constraint on the melt.

Two apparent inconsistencies with prior literature were observed in the current study. First, Alizadeh et al. observed a decrease in $T_{r,w}$ with increasing SCB content,[45] hence similar values, differing by just 2 °C, for L152 and H4 would be unexpected (Figure 3.8). Second, reversible crystallinity has been observed to account for more of the

total X_c as SCB increases,[45, 75, 79] yet again L152 and H4 are unexpectedly similar (difference between circles and squares in Figure 3.8). However, Alizadeh et al. compared samples with a greater variation of SCB content. A difference of approximately 20 °C in $T_{r,w}$ was observed between samples that differed in comonomer content by 9 mol % (Figure 5 of ref. 45). In contrast, L152 and H4 only differ by 1.4 mol % comonomer, for which we could estimate an expected difference in $T_{r,w}$ of 2-3 °C and little change in the reversible fraction, consistent with our observations.

3.4.3.2 Long Period

The transition to reversible behavior of the long period occurs at similar values of L_p for the HPBD materials studied (15.5 ± 1 nm; filled squares in Figure 3.11). This observation suggests that $T_{r,s}$ is dictated by the distribution of the lamellar crystals. The temperature at which each material develops this similar morphology that can only support fringed micelle formation ($T_{r,s}$) depends on molecular weight and SCB content: materials with larger $M_{w,tot}$ (S3 and L152 as compared to L53) and higher SCB content (H4 as compared to L152 and S3) require cooling to lower temperatures (Figure 3.11).

Although the long period at $T_{r,s}$ is the same, the long period at T = 0 °C differs among the HPBDs (filled circles in Figure 3.11), following a similar trend as the peak crystallization temperature. Since L53 begins crystallization at a higher temperature, it initially forms a larger long period which keeps the average long period higher than that of the other materials when compared at the same temperatures. For this thermal history (cooling at 10 °C/min), molecular characteristics are found to affect lamellar formation and hence influence the final long period. In contrast, previous studies have observed a long period of approximately 15 nm independent of molecular weight (M_w > 10 kg/mol)

and SCB content (>20 SCB/1000 C) following quenching to room temperature.[44,52] This discrepancy suggests the formation of different nanostructure, likely governed by different physics, for the two thermal treatments. The work of Voigt-Martin et al. confirms differences in structure formation; the authors observed that an HPBD with a molecular weight of 108 kg/mol was able to form medium-length, curved lamellae under slow-cooled conditions, but exhibited no lamellar character subsequent to quenching.[101] Additionally, Goderis et al. demonstrated that crystal thickness is greater in ethylene-co-octene samples that were slowly cooled compared to quenched.[88] During quenching, the majority of crystallization occurs from neighboring ethylene sequences having insufficient time to find most stable conformations. In contrast, crystallization during cooling ramps (even at 10 °C/min) provides adequate time for crystallization occurring from ethylene sequences of intermediate length, and hence, a greater effect of molecular characteristics is observed.

3.4.3.3 DSC Crystallization Kinetics

In the present study, the long-chain branched (LCB) molecules (S3 and H4) exhibited only slightly slower kinetics than linear samples; strong differences can be attributed to increased molecular weight (S3 vs. L53) and short-chain branching content (H4 vs. L152).[29, 30, 33-37, 44] The strong effect of long-chain branching on crystallization kinetics, expected based on prior literature, was *not* observed.[4, 68, 69] Although some qualitative agreement was seen with the work of Haigh et al.,[68] the conclusions reached here are quite different. In their work, Haigh et al. studied a short linear HPBD and a star HPBD similar to the ones examined here and observed the same relative behavior (i.e., the 3-arm star crystallized much slower than the linear polymer having molecular weight matching

one of the arms; see Figure 3.4). The authors argued that the crystallizing entities of the two polymers were the same (since the branch point cannot crystallize), and hence, the strong decrease in crystallization kinetics was attributed to long-chain branching. However, here, we were able to compare a star polymer to a linear HPBD of similar molecular weight and SCB content. The nearly identical thermal behavior of the two materials indicates that one long chain branch has negligible effect.

Similar crystallization kinetics between L152 and S3 indicate that melt dynamics do not dictate crystallization of random copolymers. L152 exhibits relaxation behavior that scales as a power law with its molecular weight.[102] In contrast, the star polymer relaxes by arm retraction and has relaxation times that scale exponentially with the molecular weight of the arms.[103] Therefore, despite the three-fold difference between $M_{w,a}$ for the star and $M_{w,tot}$ for the long linear polymer, the relaxation time of the star is significantly slower. The profound difference in melt dynamics yet nearly identical crystallization kinetics is another example of a principle difference between random copolymers and homopolymers. While crystallization kinetics of random copolymers are primarily dictated by molecular weight, this effect is not a consequence of melt dynamics, but rather because $M_{w,tot}$ dictates the amount of chain pinning to crystal surfaces.

3.4.4 Implications for Flow-Induced Crystallization

While a few long-chain branches have negligible effect on quiescent crystallization, their effect on the relaxation time of a molecule becomes important when exposed to a flow field. As relaxation time increases with LCB content,[13, 14, 104] molecules have a greater response to the flow field, allowing the for formation of oriented nuclei,[11, 105]

which enhance crystallization kinetics and result in oriented morphology. [3, 4, 8, 105] Therefore, the ultimate material properties of processed semicrystalline polymers, which are directly related to morphology, are highly dependent upon the slow-relaxing molecules.[12, 105, 106] Model hydrogenated polybutadienes are thought to have opened the door for well-defined studies of the effects of melt dynamics on flow-induced crystallization (FIC).[3] The number and length of long-chain branches can be well-defined to systematically alter the relaxation times of these materials and can be used control the morphology formation subsequent to flow.[107, 108]

We conducted preliminary studies to probe the effects of melt dynamics on flow-induced crystallization (FIC) by examining a bimodal system containing a small concentration of a slow-relaxing species in the form of a model comb polymer blended with fast-relaxing matrix (short, linear copolymer). The bimodal components were selected to have matching SCB content in order to specifically isolate the effect of long-chain branches. Details of the experiment are provided in Thesis Appendix B. Contrary to our expectations, neither increased crystallization kinetics nor preferred orientation was observed. This surprising result suggests that even under flow, short-chain branching significantly hinders crystallization. The effect of short-chain branching on FIC is explored in Chapter 5.

3.5 CONCLUSION

The study of model hydrogenated polybutadienes (HPBDs) of complex architecture revealed that the interplay between long-chain and short-chain branches is dominated by the ethylene sequence length distribution (ESLD). Differences in thermal and morpho-

logical behavior observed between (1) a short, linear chain, (2) a long, linear chain, (3) a star-polymer, and (4) an H-polymer are primarily explained by differences in SCB content and molecular weight. This is also the case for crystallization kinetics, which have previously been reported to be strongly dependent on long-chain branching.[68] Nearly identical crystallization kinetics observed between materials having significant differences in melt dynamics, highlights the importance of ESLD in the crystallization of random copolymers. Even in the presence of a flow field, oriented crystallization in the presence of a slow-relaxing comb polymer was suppressed, indicating the dominance of SCB content.

The evolution of morphology in SCB systems was examined both during temperature ramps and under isothermal conditions. During temperature ramps, three temperature regions defined by specific morphology development were identified:

(1) The 'primary-irreversible' regime is characterized by rapid, irreversible crystallization at relatively high temperatures via the propagation of primary lamellae in an unconstrained melt.

(2) The 'secondary-irreversible' regime is characterized by slower, irreversible crystallization at intermediate temperatures via the formation of secondary lamellae in constrained melt between previously-formed lamellae having the largest non-crystalline regions.

(3) The 'reversible' crystallization regime is characterized by slow, reversible crystallization at low temperatures via the formation of fringed micelles between pre-existing crystals.

In light of these regimes, double melting behavior observed by DSC subsequent

to isothermal crystallization is explained by the melting of primary and secondary lamellae. The high-melting peak ($T_{m,high}$) is attributed to the same rapidly-crystallizing, primary lamellae that form at the highest temperature during cooling ramps (primary-irreversible regime). These primary lamellae form both during cooling to and at the isothermal crystallization temperature (T_c). Given that the isothermal temperature used in these, as well as in many other studies,[44, 45, 55, 62, 109] is in the irreversible regime, the low-melting peak ($T_{m,low}$) is attributed to the melting of secondary lamellae—and not fringed micelles—that form from ethylene sequences whose length, and hence thermal stability, is dictated by T_c.

The effect of the heterogeneous morphology in copolymers is manifested as dynamic SAXS and WAXS data obtained during crystallization. This data is well suited for a prevalent technique in the field of vibrational spectroscopy to examine changes in spectra as a function of a perturbation variable, such as temperature or time. Two-dimensional correlation analysis is used in the following chapter in order to further examine morphology development and explore questions regarding the presence of an intermediate phase and the onset of crystallization.

3.6 APPENDIX—Crystalline and Amorphous Layer Thickness

For an ideal, two-phase system, it is possible to estimate the crystalline and amorphous layer thicknesses (L_c and L_a, respectively) from the long period (L_p) and volume fraction crystallinity (φ_1). Volume fraction crystallinity for each material was estimated from X_c by taking the density of purely crystalline PE to be 1.0 g/cm^3 and that of amorphous PE to be 0.855 g/cm^3.[110, 111] Hence,

$$L_c = L_p\varphi_1, \tag{3.3}$$

and

$$L_a = L_p(1 - \varphi_1). \tag{3.4}$$

We acknowledge that this analysis is not rigorous due to both the assumption of a two-phase model[112] and the fact that SAXS and WAXS are sensitive to different morphological features: WAXS identifies crystalline unit cells, and SAXS arises as the result of electron density contrast.[67, 113-115] However, a number of qualitative observations from this analysis are useful for elucidating the morphology.

This analysis indicates that the decrease in the long period during cooling is the result of a strong decrease in the apparent thickness of the amorphous layer (Figure 3.18). The crystalline layer thickness remains relatively constant with decreasing temperature, in agreement with past literature.[48, 79, 88, 90] From Figure 3.18, it is apparent that the temperature of the transition to reversible behavior is dominated by the amorphous layer. Below this transition temperature (shaded region in Figure 3.18), estimated L_a and L_c values are invalid, since we do not expect formation of lamellae in this region. Additionally, the crystalline layer exhibited reversible behavior with little change at temperatures below

the primary crystallization temperature, as determined by DSC ($T_{x,high}$). For all HPBD materials, the amorphous layer was thicker than the crystalline layer at all temperature examined and dominated L_p behavior.

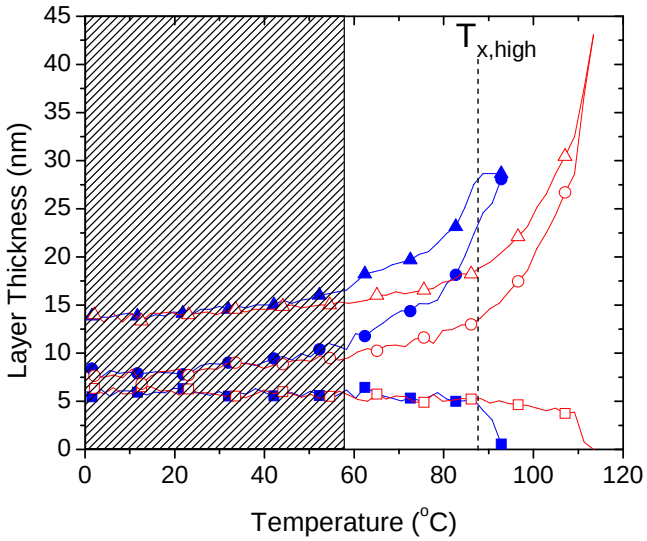

Figure 3.18 Long period (L_p, triangles), crystalline (L_c, squares) and amorphous (L_a, circles) layer thicknesses of L152 during cooling (solid symbols) and subsequent heating (open symbols) at 10 °C/min.

3.7 ACKNOWLEDGEMENTS

This work would not have been possible without ExxonMobil Research and Engineering Company (Clinton, NJ), particularly Dr. David Lohse, Dr. Cynthia Mitchell, Dr. Manika Varma-Nair, Dr. Lisa Baugh and the rest of the team, who provided financial support, experimental assistance, and fruitful discussions. The materials examined here were graciously synthesized by Prof. Nikos Hadjichristidis (University of Athens, Athens, Greece) and made available through collaboration with ExxonMobil. Additionally, we would like to thank Dr. Soo-Young Park (Kyunpook National University, Daegu, South Korea) and Robert Panepinto (ExxonMobil) for conducting DSC studies. We must thank the beamline staff at beamline X27C at NSLS BNL (Dr. Lixia Rong and Jie Zhu) and at

beamline 7.3.3 at ALS LBL (Dr. Alexander Hexemer and Eliot Gann). X-ray data was collected with the assistance of Zuleikha Kurji (Caltech). Finally, we would like to thank Prof. Rufina Alamo and Madhavi Vadlama (Florida State University) for fruitful discussions and their aid in the visualization of polymer morphology. Part of this work was funded by the National Science Foundation (DMR-0505393 and GOALI-0523083). Manuscript preparation was assisted by Prof. Julia Kornfield (Caltech), Oliver W. Bucci-cone (Tanner Research, Monrovia, CA), Havala O.T. Pye (Caltech), and Mary Louie (Caltech).

3.8 REFERENCES

1. Gahleitner, M., Melt rheology of polyolefins. *Progress in Polymer Science* **2001,** 26, (6), 895-944.
2. Wood-Adams, P. M.; Dealy, J. M.; deGroot, A. W.; Redwine, O. D., Effect of molecular structure on the linear viscoelastic behavior of polyethylene. *Macromolecules* **2000,** 33, (20), 7489-7499.
3. Heeley, E. L.; Fernyhough, C. M.; Graham, R. S.; Olmsted, P. D.; Inkson, N. J.; Embery, J.; Groves, D. J.; McLeish, T. C. B.; Morgovan, A. C.; Meneau, F.; Bras, W.; Ryan, A. J., Shear-induced crystallization in blends of model linear and long-chain branched hydrogenated polybutadienes. *Macromolecules* **2006,** 39, 5058-5071.
4. Bustos, F.; Cassagnau, P.; Fulchiron, R., Effect of molecular architecture on quiescent and shear-induced crystallization of polyethylene. *Journal of Polymer Science Part B - Polymer Physics* **2006,** 44, (11), 1597-1607.
5. Agarwal, P. K.; Somani, R. H.; Weng, W.; Mehta, A.; Yang, L.; Ran, S.; Liu, L.; Hsiao, B. S., Shear-Induced Crystallization in Novel Long Chain Branched Polypropylenes by in Sity Rheo-SAXS and -WAXD. *Macromolecules* **2003,** 36, 5226-5235.
6. Nogales, A.; Hsiao, B. S.; Somani, R. H.; Srinivas, S.; Tsou, A. H.; Balta-Calleja, F. J.; Ezquerra, T. A., Shear-induced crystallization of isotactic polypropylene with different molecular weight distributions: in situ small- and wide-angle X-ray scattering studies. *Polymer* **2001,** 42, (12), 5247-5256.
7. Fernandez-Ballester, L. Formation of oriented precursors in flow-induced polymer crystallization: experimental methods and model materials. California Institute of Technology, Pasadena, CA, 2007.
8. Kumaraswamy, G.; Kornfield, J. A.; Yeh, F.; Hsiao, B. S., Shear-Enhanced Crystallization in Isotatctic Polypropylene. 3. Evidence for a Kinetic Pathway to Nucleation.

Macromolecules **2002,** 35, 1762-1769.

9. Bond, E. B.; Spruiell, J. E., Melt spinning of metallocene catalyzed polypropylenes. I. On-line measurements and their interpretation. *Journal of Applied Polymer Science* **2001,** 82, (13), 3223-3236.
10. Liedauer, S.; Eder, G.; Janeschitz-Kriegl, H.; Jerschow, P.; Geymayer, W.; Ingolic, E., On the kinetics of shear-induced crystallization in polypropylene. *International Polymer Processing* **1993,** 8, (3), 236-244.
11. Kumaraswamy, G., Crystallization of Polymers from Stressed Melts. *Journal of Macromolecular Science, Part C: Polymer Reviews* **2005,** 45, 375-397.
12. Somani, R. H.; Yang, L.; Zhu, L.; Hsiao, B. S., Flow-induced shish-kebab precursor structures in entangled polymer melts

Polymer **2005,** 46, 8587-8623.

13. McLeish, T. C. B., Hierarchical-relaxation in tube models of branched polymers. *Europhysics Letters* **1988,** 6, (6), 511-516.
14. Kapnistos, M.; Vlassopoulos, D.; Roovers, J.; Leal, L. G., Linear Rheology of Architecturally Complex Macromolecules: Comb Polymers with Linear Backbones. *Macromolecules* **2005,** 38, 7852-7862.
15. Malmberg, A.; Kokko, E.; Lehmus, P.; Lofgren, B.; Seppala, J. V., Long-chain branched polyethene polymerized by metallocene catalysts Et[Ind](2)ZrCl2/MAO and Et[IndH(4)](2)ZrCl2/MAO. *Macromolecules* **1998,** 31, (24), 8448-8454.
16. Shiono, T.; Azad, S. M.; Ikeda, T., Copolymerization of atactic polypropene macromonomer with propene by an isospecific metallocene catalyst. *Macromolecules* **1999,** 32, (18), 5723-5727.
17. Mehdiabadi, S.; Soares, J. B. P.; Dekmezian, A. H., Production of Long-Chain Branched Polyolefins with Two Single-Site Catalysts: Comparing CSTR and Semi-Batch Performance. *Macromolecular Reaction Engineering* **2008,** 2, (6), 529-550.

18. Schwerdtfeger, E. D.; Irwin, L. J.; Miller, S. A., Highly branched polyethylene from ethylene alone via a single zirconium-based catalyst. *Macromolecules* **2008,** 41, (4), 1080-1085.
19. Lofgren, B.; Kokko, E.; Seppala, J., Specific structures enabled by metallocene catalysis in polyethenes. In *Long-Term Properties of Polyolefins*, Springer-Verlag Berlin: Berlin, 2004; Vol. 169, pp 1-12.
20. Wood-Adams, P. M.; Dealy, J. M., Using rheological data to determine the branching level in metallocene polyethylenes. *Macromolecules* **2000,** 33, (20), 7481-7488.
21. Alamo, R. G.; Mandelkern, L., The crystallization behavior of random copolymers of ethylene. *Thermochimica Acta* **1994,** 238, 155-201.
22. Hadjichristidis, N.; Xenidou, M.; Iatrou, H.; Pitsikalis, M.; Poulos, Y.; Avgeropoulos, A.; Sioula, S.; Paraskeva, S.; Velis, G.; Lohse, D. J.; Schulz, D. N.; Fetters, L. J.; Wright, P. J.; Mendelson, R. A.; Garcia-Franco, C. A.; Sun, T.; Ruff, C. J., Well-defined, model long chain branched polyethylene. 1. Synthesis and characterization. *Macromolecules* **2000,** 33, (7), 2424-2436.
23. Bender, J. T.; Knauss, D. M., Synthesis of Low Polydispersity Polybutadiene and Polyethylene Stars by Convergent Living Anionic Polymerization. *Journal of Polymer Science: Part A: Polymer Chemistry* **2006,** 44, 828-836.
24. Driva, P.; Iatrou, H.; Lohse, D. J.; Hadjichristidis, N., Anionic Homo-and Copolymerization of Double-Tailed Macromonomers: A Route to Novel Macromolecular Architectures. *Journal of Polymer Science: Part A: Polymer Chemistry* **2005,** 43, 4070-4078.
25. Koutalas, G.; Iatrou, H.; Lohse, D. J.; Hadjichristidis, N., Well-Defined Comb, Star-Comb, and Comb-on-Comb Polybutadienes by Anionic Polymerization and the Macronomer Strategy. *Macromolecules* **2005,** 38, 4996-5001.
26. Vazaios, A.; Lohse, D. J.; Hadjichristidis, N., Linear and Star Block Copolymers of

Styrenic Macromoners by Anionis Polymerization. *Macromolecules* **2005,** 38, 5468-5474.

27. Rachapudy, H.; Smith, G. G.; Raju, V. R.; Graessley, W. W., Properties of Amorphous and Crystallizable Hydrocarbon Polymers .3. Studies of the Hydrogenation of Polybutadiene. *Journal of Polymer Science Part B-Polymer Physics* **1979,** 17, (7), 1211-1222.
28. Krigas, T. M.; Carella, J. M.; Struglinski, M. J.; Crist, B.; Graessley, W. W.; Schilling, F. C., Model Copolymers of Ethylene with Butene-1 Made by Hydrogenation of Polybutadiene - Chemical Composition and Selected Physical Properities. *Journal of Polymer Science: Part B: Polymer Physics* **1985,** 23, (3), 509-520.
29. Cerrada, M. L.; Benavente, R.; Perez, E., Influence of thermal history on morphology and viscoelastic behavior of ethylene-1-octene copolymers synthesized with metallocene catalysts. *Journal of Materials Research* **2001,** 16, (4), 1103-1111.
30. Peeters, M.; Goderis, B.; Vonk, C.; Reynaers, H.; Mathot, V., Morphology of Homogeneous Copolymers of Ethene and 1-Octene. I. Influence of Thermal History on Morphology. *Journal of Polymer Science: Part B: Polymer Physics* **1997,** 35, 2689-2713.
31. Krishnaswamy, R. K.; Yang, Q.; Fernandez-Ballester, L.; Kornfield, J. A., Effect of the distribution of short-chain branches on crystallization kinetics and mechanical properties of high-density polyethylene. *Macromolecules* **2008,** 41, (5), 1693-1704.
32. Bensason, S.; Minick, J.; Moet, A.; Chum, S.; Hiltner, A.; Baer, E., Classification of Homogeneous Ethylene-Octene Copolymers Based on Comonomer Content. *Journal of Polymer Science: Part B: Polymer Physics* **1996,** 34, 1301-1315.
33. Simanke, A. G.; Alamo, R. G.; Galland, G. B.; Mauler, R. S., Wide-angle X-ray scattering of random metallocene-ethylene copolymers with different types and concentration of comonomer. *Macromolecules* **2001,** 34, (20), 6959-6971.

34. Alamo, R.; Domszy, R.; Mandelkern, L., Thermodynamic and Structural-Properties of Copolymers of Ethylene. *Journal of Physical Chemistry* **1984,** 88, (26), 6587-6595.

35. Alamo, R. G.; Mandelkern, L., Crystallization Kinetics of Random Ethylene Copolymers. *Macromolecules* **1991,** 24, 6480-6493.

36. Stadler, F. J.; Takahashi, T.; Yonetake, K., Crystallite dimensions - characterization of ethene-/alpha-olefin Copolymers with various comonomers and comonomer Ccontents measured by small- and wide angle X-ray scattering. *E-Polymers* **2009**, 19.

37. Mathot, V. B. F.; Scherrenberg, R. L.; Pijpers, T. F. J. In *Metastability and order in linear, branched and copolymerized polyethylenes*, 1998; Elsevier Sci Ltd: 1998; pp 4541-4559.

38. Mandelkern, L.; Glotin, M.; Benson, R. A., Supermolecular Structure and Thermodynamic Properties of Linear and Branched Polyethylene under Rapid Crystallization Conditions. *Macromolecules* **1981,** 14, 22-34.

39. Alamo, R. G.; Viers, B. D.; Mandelkern, L., Phase-Structure of Random Ethylene Copolymers - a Study of Counit Content and Molecular-Weight as Independent Variables. *Macromolecules* **1993,** 26, (21), 5740-5747.

40. Shirayam.K; Watabe, H.; Kita, S., Effects of Branching on Some Properties of Ethylene Alpha-Olefin Copolymers. *Makromolekulare Chemie* **1972,** 151, (JAN20), 97-&.

41. Richardson, M. J.; Flory, P. J.; Jackson, J. B., Crystallization and Melting of Copolymers of Polymethylene. *Polymer* **1963,** 4, (2), 221-236.

42. Laupretre, F.; Monnerie, L.; Barthelemy, L.; Vairon, J. P.; Sauzeau, A.; Roussel, D., Influence of Crystallization Conditions on the Location of Side-Chain Branches in Ethylene Copolymers as Studied by High-Resolution Solid-State C-13 Nmr. *Polymer Bulletin* **1986,** 15, (2), 159-164.

43. Crist, B.; Williams, D. N., Crystallization and melting of model ethylene-butene ran-

dom copolymers: Thermal studies. *Journal of Macromolecular Science-Physics* **2000,** B39, (1), 1-13.

44. Alamo, R. G.; Chan, E. K. M.; Mandelkern, L.; Voigt-Martin, I. G., Influence of Molecular Weight on the Melting and Phase Structure of Random Copolymers of Ethylene. *Macromolecues* **1992,** 25, (24), 6381-6394.
45. Alizadeh, A.; Richardson, L.; Xu, J.; McCartney, S.; Marand, H.; Cheung, Y. W.; Chum, S., Influence of Structural and Topological Constraints on the Crystallization and Melting Behavior of Polymers. 1. Ethylene/1-Octene Copolymers. *Macromolecues* **1999,** 32, 6221-6235.
46. Alamo, R. G.; Mandelkern, L., Thermodynamic and Structural-Properties of Ethylene Copolymers. *Macromolecules* **1989,** 22, (3), 1273-1277.
47. Liu, W. D.; Yang, H. L.; Hsiao, B. S.; Stein, R. S.; Liu, S. S.; Huang, B. T. In *Real-time crystallization and melting study at ethylene-based copolymers by SAXS, WAXD, and DSC techniques*, 2000; Cebe, P.; Hsiao, B. S.; Lohse, D. J., Eds. Amer Chemical Soc: 2000; pp 187-200.
48. Vanden Eynde, S.; Mathot, V.; Koch, M. H. J.; Reynaers, H., Thermal behaviour and morphology of homogeneous ethylene-propylene and ethylene-1-butene copolymers with high comonomer contents. *Polymer* **2000,** 41, (9), 3437-3453.
49. Howard, P. R.; Crist, B., Unit-Cell Dimensions in Model Ethylene Butene-1 Copolymers. *Journal of Polymer Science Part B-Polymer Physics* **1989,** 27, (11), 2269-2282.
50. Mathot, V. B. F.; Pijpers, M. F. J., Molecular-Structure, Melting Behavior, and Crystallinity of 1-Octene-Based Very Low-Density Polyethylenes (Vldpes) as Studied by Fractionation and Heat-Capacity Measurements with Dsc. *Journal of Applied Polymer Science* **1990,** 39, (4), 979-994.
51. Flory, P. J., Theory of Crystallization in Copolymers. *Transactions of the Faraday*

Society **1955,** 51, (6), 848-857.

52. Crist, B.; Howard, P. R., Crystallization and Melting of Model Ethylene-Butene Copolymers. *Macromolecules* **1999,** 32, 3057-3067.
53. Kolesov, I. S.; Androsch, R.; Radusch, H. J. In *Non-isothermal crystallization of polyethylenes as function of cooling rate and concentration of short chain branches*, 2004; Kluwer Academic Publ: 2004; pp 885-895.
54. Wunderlich, B., *Macromolecular Physics*. Academic Press: New York, 1999; Vol. 3.
55. Crist, B.; Claudio, E. S., Isothermal crystallization of random ethylene-butene copolymers: Bimodal kinetics. *Macromolecules* **1999,** 32, (26), 8945-8951.
56. Rabiej, S.; Goderis, B.; Janicki, J.; Mathot, V. B. F.; Koch, M.; Reynaers, H.; Wlochowicz, A. In *Influence of thermal treatment on the supermolecular structure of homoueneous polyethylene-1-octene copolymers*, 2003; Inst Chemical Fibres: 2003; pp 28-31.
57. Minick, J.; Moet, A.; Hiltner, A.; Baer, E.; Chan, S. P., Crystallization of Very-Low-Density Copolymers of Ethylene With Alpha-Olefins. *Journal of Applied Polymer Science* **1995,** 58, (8), 1371-1384.
58. Wang, C.; Chu, M. C.; Lin, T. L.; Lai, S. M.; Shih, H. H.; Yang, J. C., Microstructures of a highly short-chain branched polyethylene. *Polymer* **2001,** 42, (4), 1733-1741.
59. Okui, N.; Kawai, T., Crystallization of Ethylene/Vinylacetate Random Copolymers. *Makromolekulare Chemie* **1972,** 154, (NAPR), 161-&.
60. Qiu, J.; Xu, D.; Zhao, J.; Niu, Y.; Wang, Z., New Insights into the Multiple Melting Behaviors of the Semicrystalline Ethylene-Hexene Copolymer: Origins of Quintuple Melting Peaks. *Journal of Polymer Science: Part B: Polymer Physics* **2008,** 46, 2100-2115.
61. Zhang, F. J.; Liu, J. P.; Xie, F. C.; Fu, Q.; He, T. B., Polydispersity of ethylene se-

quence length in metallocene ethylene/alpha-olefin copolymers. II. Influence on crystallization and melting behavior. *Journal of Polymer Science Part B-Polymer Physics* **2002,** 40, (9), 822-830.

62. Rabiej, S.; Goderis, B.; Janicki, J.; Mathot, V. B. F.; Koch, M. H. J.; Groeninckx, G.; Reynaers, H.; Gelan, J.; Wlochowicz, A., Characterization of the dual crystal population in an isothermally crystallized homogeneous ethylene-1-octene copolymer. *Polymer* **2004,** 45, 8761-8778.
63. The author would like to thank Lixia Rong and Jie Zhu with beamline assistance.
64. The author would like to thank Eliot Gann and Alexander Hexemer with beamline assistance, as well as Zuleikha Kurji for aid in conducting experiments.
65. Cser, F., About the Lorentz correction used in the interpretation of small angle X-ray scattering data of semicrystalline polymers. *Journal of Applied Polymer Science* **2001,** 80, (12), 2300-2308.
66. Goderis, B.; Reynaers, H.; Koch, M. J., Primary and Secondary Crystallization in a Homogeneous Ethylene-1-Octene Copolymer: Crystallinity Heterogeneity Studied by SAXS. *Macromolecules* **2002,** 25, 5840-5853.
67. Mathot, V. B. F.; Scherrenberg, R. L.; Pijpers, M. F. J.; Bras, W., Dynamic DSC, SAXS and WAXS on homogeneous ethylene-propylene and ethylene-octene copolymers with high comonomer contents. *Journal of Thermal Analysis* **1996,** 46, (3-4), 681-718.
68. Haigh, J. A.; Nguyen, C.; Alamo, R. G.; Mandelkern, L., CRYSTALLIZATION AND MELTING OF MODEL POLYETHYLENES WITH DIFFERENT CHAIN STRUCTURES. *Journal of Thermal Analysis and Calorimetry* **2000,** 59, 435-440.
69. Isasi, J. R.; Haigh, J. A.; Graham, J. T.; Mandelkern, L.; Alamo, R. G. In *Some aspects of the crystallization of ethylene copolymers*, 2000; Elsevier Sci Ltd: 2000; pp 8813-8823.

70. Peng, Y.; Fu, Q.; Chiu, F.-C., Crystallization and morphology of metallocene polyethylenes with well-controlled molecular weight and branching content. *Polymer International* **2003,** 52, 164-171.

71. Hoffman, J. D.; Weeks, J. J., Melting Process and Equilibrium Melting Temperature of Polychlorotrifluoroethylene. *Journal of Research of the National Bureau of Standards Section a-Physics and Chemistry* **1962,** 66, (JAN-F), 13-&.

72. Mandelkern, L., The Dependence of the Melting Temperature of Bulk Homopolymers on the Crystallization Temperature. *Journal of Polymer Science* **1960,** 47, (0149), 494-496.

73. Kim, M. H.; Phillips, P. J.; Lin, J. S., The equilibrium melting points of random ethylene-octene copolymers: A test of the Flory and Sanchez-Eby theories. *Journal of Polymer Science Part B-Polymer Physics* **2000,** 38, (1), 154-170.

74. Lorenzo, A. T.; Arnal, M. L.; Muller, A. J.; de Fierro, A. B.; Abetz, V., High speed SSA thermal fractionation and limitations to the determination of lamellar sizes and their distributions. *Macromolecular Chemistry and Physics* **2006,** 207, (1), 39-49.

75. Androsch, R.; Wunderlich, B., Specific reversible melting of polyethylene. *Journal of Polymer Science Part B-Polymer Physics* **2003,** 41, (18), 2157-2173.

76. Nam, J. Y.; Kadomatsu, S.; Saito, H.; Inoue, T., Thermal reversibility in crystalline morphology of LLDPE crystallites. *Polymer* **2002,** 43, (7), 2101-2107.

77. Schultz, J. M.; Fischer, E. W.; Schaumburg, O.; Zachmann, H. A., Small-Angle X-Ray-Scattering Studies of Melting. *Journal of Polymer Science Part B-Polymer Physics* **1980,** 18, (2), 239-245.

78. Androsch, R.; Wunderlich, B., Analysis of the degree of reversibility of crystallization and melting in poly(ethylene-co-1-octene). *Macromolecules* **2000,** 33, (24), 9076-9089.

79. Joubert, D. J.; Goderis, B.; Reynaers, H.; Mathot, V. B. F., Spatially inhomogeneous

crystallinity in heterogeneous ethylene-alpha-olefin copolymers. *Journal of Polymer Science Part B-Polymer Physics* **2005,** 43, (21), 3000-3018.

80. Strobl, G. R.; Schneider, M. J.; Voigtmartin, I. G., Model of Partial Crystallization and Melting Derived from Small-Angle X-Ray-Scattering and Electron-Microscopic Studies on Low-Density Polyethylene. *Journal of Polymer Science Part B-Polymer Physics* **1980,** 18, (6), 1361-1381.
81. Li, Y.; Akpalu, Y. A., Probing the Melting Behavior of a Homogeneous Ethylene/1-Hexene Copolymer by Small-Angle Light Scattering. *Macromolecules* **2004,** 27, 7265-7277.
82. Schouterden, P.; Vandermarliere, M.; Riekel, C.; Koch, M. H. J.; Groeninckx, G.; Reynaers, H., Characterization of the Morphological-Changes in Linear Low-Density Polyethylene During the Melting Process Using Synchrotron Radiation. *Macromolecules* **1989,** 22, (1), 237-244.
83. Vonk, C. G.; Koga, Y., An X-Ray-Diffraction Study of Nonlinear Polyethylene .2. Small-Angle Scattering Observations near the Melting-Point. *Journal of Polymer Science Part B-Polymer Physics* **1985,** 23, (12), 2539-2548.
84. Akpalu, Y. A.; Amis, E. J., Evolution of density fluctuations to lamellar crystals in linear polyethylene. *Journal of Chemical Physics* **1999,** 111, (18), 8686-8695.
85. Bark, M.; Zachmann, H. G.; Alamo, R.; Mandelkern, L., Investigations of the Crystallization of Polyethylene by Means of Simultaneous Small-Angle and Wide-Angle X-Ray-Scattering. *Makromolekulare Chemie-Macromolecular Chemistry and Physics* **1992,** 193, (9), 2363-2377.
86. Chiu, F. C.; Wang, Q.; Fu, Q.; Honigfort, P.; Cheng, S. Z. D.; Hsiao, B. S.; Yeh, F. J.; Keating, M. Y.; Hsieh, E. T.; Tso, C. C., Structural and morphological inhomogeneity of short-chain branched polyethylenes in multiple-step crystallization. *Journal of Macromolecular Science-Physics* **2000,** B39, (3), 317-331.

87. Xu, J. T.; Li, B. T.; Fan, Z. Q.; Ryan, A. J., Simultaneous SAXS/WAXS/DSC studies on microstructure of conventional and metallocene-based ethylene-butene copolymers. *Chinese Journal of Polymer Science* **2004,** 22, (3), 279-287.

88. Goderis, B. In *Thermal behaviour and real-time morphology of polyolefin systems*, 2003; Inst Chemical Fibres: 2003; pp 14-19.

89. Rabiej, S., On the origin of the multiple melting observed after isothermal crystallization of homogeneous ethylene/1-octene copolymers. *Polimery* **2004,** 49, (6), 414-423.

90. Janicki, J. In *SAXS and WAXD real time studies on nanostructure of selected polymer materials*, 2004; Elsevier Science Sa: 2004; pp 61-67.

91. Wang, Z.; Wang, H.; Shimizu, K.; Dong, K.-Y.; Hsiao, B. S.; Han, C. C., Structural and morphological development in poly(ethylene-co-hexene) and poly(ethylene-co-butylene) blends due to the competition between liquid-liquid phase separation and crystallization. *Polymer* **2005,** 46, 2675-2684.

92. Sajkiewicz, P.; Hashimoto, T.; Saijo, K.; Gradys, A., 'Intermediate phase' in poly(ethylene) as elucidated by the WAXS. Analysis of crystallization kinetics. *Polymer* **2005,** 46, (2), 513-521.

93. Baker, A. M. E.; Windle, A. H., Evidence for a partially ordered component in polyethylene from wide-angle X-ray diffraction. *Polymer* **2001,** 42, (2), 667-680.

94. McFaddin, D. C.; Russell, K. E.; Wu, G.; Heyding, R. D., Characterization of Polyethylenes by X-Ray-Diffraction and C-13-Nmr - Temperature Studies and the Nature of the Amorphous Halo. *Journal of Polymer Science Part B-Polymer Physics* **1993,** 31, (2), 175-183.

95. Monar, K.; Habenschuss, A. In *Modeling the principal amorphous halo in quiescent melts of polyethylene and ethylene copolymers using wide-angle X-ray scattering and its implications*, 1999; John Wiley & Sons Inc: 1999; pp 3401-3410.

96. Russell, K. E.; Hunter, B. K.; Heyding, R. D., Polyethylenes Revisited - Waxs and

the Phase-Structure. *European Polymer Journal* **1993,** 29, (2-3), 211-217.

97. Wunderlich, B., Reversible crystallization and the rigid-amorphous phase in semicrystalline macromolecules. *Progress in Polymer Science* **2003,** 28, (3), 383-450.
98. Janimak, J. J.; Stevens, G. C., Comparative crystallisation and exploratory micro-structure studies of novel polyethylenes with tailored molecular characteristics. *Polymer* **2000,** 41, (11), 4233-4248.
99. Akpalu, Y.; Kielhorn, L.; Hsiao, B. S.; Stein, R. S.; Russell, T. P.; Egmond, J. v.; Muthukumar, M., Structure Development during Crystallization of Homogeneous Copolymers of Ethene and 1-Octene: Time-Resolved Synchrotron X-ray and SALS Measurements. *Macromolecules* **1999,** 32, 765-770.
100. Mirabella, F. M., Crystallization and melting of narrow composition distribution polyethylenes: Investigation and implications of crystal thickening. *Journal of Polymer Science Part B-Polymer Physics* **2003,** 41, (3), 235-246.
101. Voigt-Martin, I. G.; Alamo, R.; Mandelkern, L., A Quantitative Electron-Microscopic Study of the Crystalline-Structure of Ethylene Copolymers. *Journal of Polymer Science Part B-Polymer Physics* **1986,** 24, (6), 1283-1302.
102. Doi, M.; Edwards, S. F., *The Theory of Polymer Dynamics*. Oxford University Press: Oxford, 1986.
103. Milner, S. T.; McLeish, T. C. B., Parameter-Free Theory for Stress Relaxation in Star Polymer Melts. *Macromolecules* **1997,** 30, 2159-2166.
104. Ferry, J. D., *Viscoelastic Properties of Polymers*. 2 ed.; Wiley: New York, 1970.
105. Seki, M.; Thurman, D. W.; Oberhauser, J. P.; Kornfield, J. A., Shear-mediated crystallization of isotatctic polypropylene: The role of long chain -- long chain overlap. *Macromolecules* **2002,** 35, 2583-2594.
106. Yang, L.; Somani, R. H.; Sics, I.; Hsiao, B. S.; Kolb, R.; Lohse, D., The role of high molecular weight chains in flow-induced crystallization precursor structures.

Journal of Physics: Condensed Matter **2006,** 18, S2421-S2436.

107. Daniels, D. R.; McLeish, T. C. B.; Kant, R.; Crosby, B. J.; Young, R. N.; Pryke, A.; Allgaier, J.; Groves, D. J.; Hawkins, R. J., Linear rheology of diluted linear, star and model long chain branched polymer melts. *Rheologica Acta* **2001,** 40, (5), 403-415.

108. Inkson, N. J.; Graham, R. S.; McLeish, T. C. B.; Groves, D. J.; Fernyhough, C. M., Viscoelasticity of monodisperse comb polymer melts. *Macromolecules* **2006,** 39, (12), 4217-4227.

109. Glotin, M.; Mandelkern, L., Crystalline Morphology of Isothermally Crystallized Branched Polyethylene. *Macromolecules* **1981,** 14, (5), 1394-1404.

110. Swan, P. R., Polyethylene Unit Cell Variations with Branching. *Journal of Polymer Science* **1962,** 56, (164), 409-&.

111. Allen, G.; Gee, G.; Wilson, G. J., Intermolecular Forces and Chain Flexibilities in Polymers .1. Internal Pressures and Cohesive Energy Densities of Simple Liquids. *Polymer* **1960,** 1, (4), 456-466.

112. Wang, Z. G.; Hsiao, B. S.; Fu, B. X.; Liu, L.; Yeh, F.; Sauer, B. B.; Chang, H.; Schultz, J. M., Correct determination of crystal lamellar thickness in semicrystalline poly(ethylene terephthalate) by small-angle X-ray scattering. *Polymer* **2000,** 41, (5), 1791-1797.

113. Peeters, M.; Goderis, B.; Reynaers, H.; Mathot, V., Morphology of Homogeneous Copolymers of Ethylene and 1-Octene. II. Structural Changes on Annealilng. *Journal of Polymer Science: Part B: Polymer Physics* **1999,** 37, (1), 83-100.

114. Vonk, C. G.; Pijpers, A. P., An X-Ray-Diffraction Study of Nonlinear Polyethylene .1. Room-Temperature Observations. *Journal of Polymer Science Part B-Polymer Physics* **1985,** 23, (12), 2517-2537.

115. Stribeck, N.; Alamo, R. G.; Mandelkern, L.; Zachmann, H. G., Study of the

Phase-Structure of Linear Polyethylene by Means of Small-Angle X-Ray-Scattering and Raman-Spectroscopy. *Macromolecules* **1995,** 28, (14), 5029-5036.